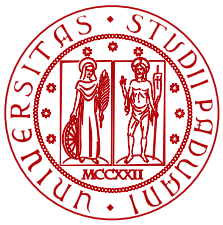

UNIVERSITÀ
DEGLI STUDI
DI PADOVA

DIPARTIMENTO
DI INGEGNERIA
DELL'INFORMAZIONE

DIPARTIMENTO DI INGEGNERIA DELL'INFORMAZIONE

CORSO DI LAUREA IN INGEGNERIA CONTROL SYSTEMS ENGINEERING

# Control of Electrically Excited Synchronous Motor


**Relatore**
Prof. Nicola Bianchi

**Laureando**
Wafeek Bader

**Correlatore**


ANNO ACCADEMICO 2023-2024


Data di laurea 03/07/2024

*Apes. Together. Strong.*

# Contents

# List of Figures

# List of Tables

**Abstract**

This master's thesis investigates the use of advanced control techniques to improve the performance and efficiency of electrically excited synchronous motors (EESMs) in a variety of industrial applications. It is worth noting that EESMs have various advantages, such as high efficiency, controllability, and robustness, making them suitable for a wide range of applications, including electric vehicles, renewable energy systems, and industrial machinery. However, it is a matter of concern to obtain optimal control solutions due to the nonlinearity of their dynamics, parameter variations, and disturbances. This thesis focuses on various advanced control strategies for Electrically Excited Synchronous Motors (EESMs) with regard to Flux Weakening, Integration Control and Optimization Issues. The study examines the development and implementation of Maximum Torque Per Ampere (MTPA), Flux Weakening, and Maximum Torque Per Voltage (MTPV) strategies for improving EESM performance and efficiency under different operational conditions.

# Chapter 1

# Introduction

## 1.1 Background

Electrically Excited Synchronous Motors (EESMs) have gained popularity in electric motor applications due to their inherent benefits. EESMs use field windings in the rotor instead of permanent magnets for field excitation, like in PMSMs [1]. This configuration provides a unique advantage: being an effective way to control the rotor field current and therefore providing a means of adjusting the motor for various needs at different operating points [2].

This implies that the control of EESMs is very important in ensuring that it operates at its best efficiency and reliability, especially when used in electric vehicles, industrial drives, and renewable energy systems where torque and speed are very important factors [3]. This thesis explores high-level control of EESMs using flux weakening control, which comprises MTPA, flux weakening, and MTPV.

## 1.2 Motivation

The growing demand for electric motors in high-performance applications necessitates control solutions to enhance EESM efficiency and torque levels. Some traditional control strategies could potentially fail to optimize the capacity of EESMs, particularly when in different loads and speeds. Flux weakening control can be identified as an effective solution to expand the operational range of the motor beyond the base speed without a negative impact on any of the characteristics [1].

MTPA, flux weakening, and MTPV control strategies help the motor to achieve high efficiency in all zones of the torque-speed plane [4]. MTPA increases the current-to-torque ratio to get the maximum torque from the system, the flux weakening enables the motor to run at a high speed by reducing the total flux, and MTPV improves the torque-to-speed control under

voltage-limited conditions [5]. These solutions provide an integrated approach to managing EESMs, improving their usability in various applications [6].

## 1.3 Objectives

This thesis aims to build and test an EESM speed control strategy combining MTPA, flux weakening, and MTPV approaches. The specific goals include:

1. Developing a control algorithm that suits the MTPA, MTPV and the flux weakening strategies. The control algorithm proposed must be incorporated into a simulation platform to assess the effectiveness of the control.

2. Evaluating the behavior of the control algorithm in various situations such as at different loads and speed settings.

3. Following the comparison between the proposed control technique and the conventional control methodologies to showcase the benefits in efficiency and torque output of the former.

## 1.4 Scope of the Thesis

The organisation of this thesis is as follows, to give an overall understanding of the control strategies of EESMs with specific attention to flux weakening control. The key areas covered include: The key areas covered include:

- **Literature Review:** The following is a discussion of the literature on control strategies in EESMs with a focus on the strengths and weaknesses of existing methodologies.

- **Theoretical Framework:** A detailed description of the functions, equations, and principles that apply to MTPA, flux weakening, and MTPV techniques.

- **Control Algorithm Design:** The synthesis of the three control approaches to produce a single control algorithm of the process, together with an explanation of how the control laws will be derived and how the control will be accomplished.

- **Simulation and Analysis:** Also, the control algorithm is implemented in a simulation environment and its performance is analyzed under various operating conditions

- **Results and Discussion:** A detailed presentation of the results, and a discussion of the implications of the findings.

- **Conclusion and Future Work:** A summary of the key contributions of the thesis, along with suggestions for future research directions.

## 1.5 Thesis Organization

The thesis is structured as follows:

### Part I: Linear Model of EESM

- **Introduction** - Provides a summary of the thesis, including background, motivation, aims, scope, and organization.
- **Theoretical Framework for Linear Model** - Explores the theoretical foundations and mathematical modeling of the EESM linear model.
- **Linear Model Control Algorithm Design** - Includes MTPA, flux weakening, and MTPV techniques.
- **Simulation and Analysis of Linear Model** - Provides simulation setup, results, and performance analysis under various operating situations.

### Part II: Nonlinear Model of EESM

- **Theoretical Framework for Nonlinear Model** - Discusses the theoretical foundations and mathematical modelling of the EESM nonlinear model.
- **Nonlinear Model Control Algorithm Design** - Details the development of the control algorithm for the nonlinear model, integrating MTPA, flux weakening, and MTPV strategies.
- **Simulation and Analysis of Nonlinear Model** - Presents the simulation setup for the nonlinear model, results, and performance analysis under various operating conditions.
- **Conclusion and Future Work** - Summarizes the key contributions of the thesis, the implications of the findings, and suggests directions for future research.

## 1.6 Summary

Research on Electrically Excited Synchronous Motors (EESMs) control is important and has the potential to improve the effectiveness and performance of many different electric motor

applications. By creating and executing a thorough control approach that combines MTPA, flux weakening, and MTPV methodologies, this thesis seeks to advance this subject. This work aims to show the effectiveness of the suggested methodology and its advantages over conventional control approaches through theoretical research, simulation, and experimental validation. The intricacies of this project will be covered in full in the upcoming chapters, which will begin with a survey of the body of research on EESM control techniques.

# Chapter 2

# Linear Model of the Motor

### 2.0.1 EESM Structure

EESM, which stands for Electrically Excited Synchronous Motor (EESM), is known for its sophisticated and extremely optimized design that ensures excellent performance and control [7]. Typically, the armature windings of the stator of EESM are located in slots made of steel laminated cores. These slots are designed to ensure distribution and management of current in a layered configuration. Mostly these windings are connected in parallel paths in order to improve efficiency and reduce electrical losses. To maximize the use of space while maintaining good insulation and thermal management, stators have precise slot dimensions that enhance both the fill factor and good insulation [8].

This sets apart EESM's rotor from other synchronous motors because it comes with field windings instead of permanent magnets. These field windings are energized by an external DC power source through slip rings and brushes, enabling the creation of a magnetic field. The latter is particularly true for wound rotor (WR) machines [7], which provide a way to increase maximum speed. Controlling the rotor flux can be done using excitation winding. As such, less voltage is needed on stator winding since lower back-electromotive force occurs on stator [9]. Also, structural elements like pole shoes and pole necks are incorporated in the rotor to assist in determining or shaping the magnetic field that is produced by windings. Furthermore, a permanent magnet can be included in the rotor to further improve on its ability to produce stronger and more stable magnetic fields.

The EESM's operation depends on how the stator and rotor magnetic fields interact. When AC current flows through stator windings, they generate a rotary magnetic field. A direct current (DC) supplied to rotor field windings creates a constant magnetic field interacting with rotating one of the stator [10]. As a result, the rotor synchronizes with this rotating magnetic Field of the stator allowing Motor to operate at a speed, which is directly proportional to the frequency of an alternating Current supply [11].

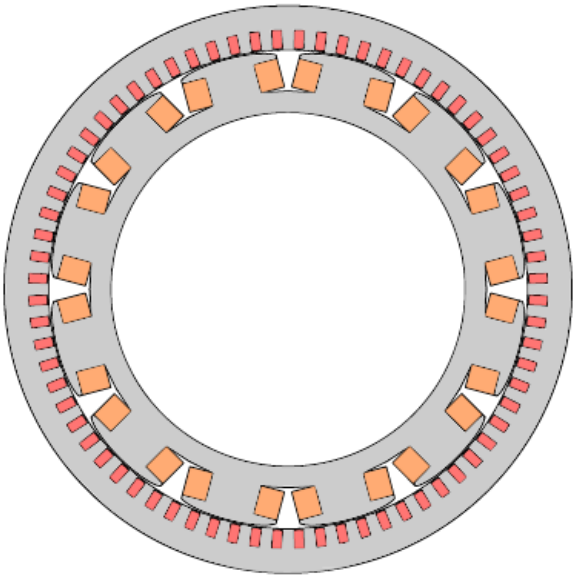

Figure 2.1: EESM Wounded Rotor Structure

Efficient magnetic coupling and minimal losses are achieved by carefully designing air gap between stator and rotor. Dynamic control of excitation current going into rotor also offers significant benefits including optimizing torque production and operational efficiency over large speed range and loads. This dynamic control capability also enables the EESM to adjust its power factor and reactive power, making it highly suitable for applications that demand precise control and high efficiency, such as in industrial drives, electric vehicles, and renewable energy systems. The robust construction and advanced control features of the EESM contribute to its reliability and performance in demanding environments [12].

### 2.0.2 Rotating dq Reference Frame

The concept of rotating the dq reference frame is one of the most basic in analyzing and controlling AC machines, including Electrically Excited Synchronous Motors (EESM). This reference frame coincides with the magnetic field of the rotor and rotates at the electrical angular speed synchronously with it [13], which is a product of motor's mechanical angular speed and its pole pairs. which rotates at the angular speed $\omega_e = p\omega_m$, where $\omega_m$ is the rotor speed and $p$ is the number of pole pairs. The direct d-axis is aligned with the rotor flux [14], and the quadrature q-axis is orthogonal to it. Under steady-state operating conditions, this transformation simplifies analysis and control of the motor by enabling conversion from three-phase stator currents and voltages to steady-state DC values in two-axis (dq) system. In this way alternating quantities are converted into constant ones during steady state operation. The d axis in the dq frame is aligned with rotor flux while q axis is perpendicular to it. It makes torque independent on

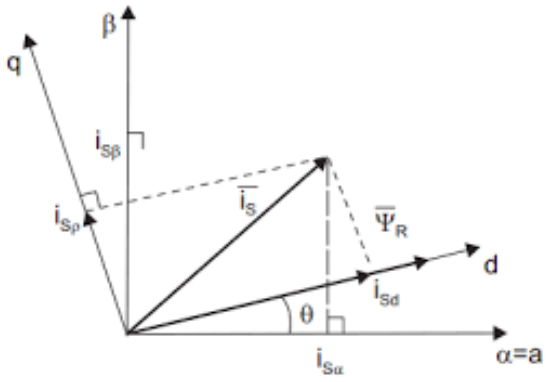


Figure 2.2: dq axis frame

flux-producing components of currents flowing through a motor thus enabling more efficient and precise control strategies such as direct torque control (DTC) and field-oriented control (FOC). Thus, torque production optimization algorithms that improve motor efficiency can be easily implemented using advanced control schemes tailored for rotating dq reference frame proposed.

The transformation from the three-phase $abc$ frame to the $dq$ frame is accomplished using the Park transformation. The transformation equations are:

$$d = \frac{2}{3}\left(i_a \cos(\theta) + i_b \cos\left(\theta - \frac{2\pi}{3}\right) + i_c \cos\left(\theta + \frac{2\pi}{3}\right)\right) \tag{2.1}$$

$$q = \frac{2}{3}\left(i_a \sin(\theta) + i_b \sin\left(\theta - \frac{2\pi}{3}\right) + i_c \sin\left(\theta + \frac{2\pi}{3}\right)\right) \tag{2.2}$$

where $i_a$, $i_b$, and $i_c$ are the phase currents and $\theta$ is the rotor electrical angle.

### 2.0.3 Voltage Equations of the Motor

In the dq reference frame, the voltage equations for the stator and rotor windings of the EESM can be expressed as follows:

$$u_d = R_s i_d + \frac{d\psi_d}{dt} - \omega_e \psi_q, \tag{2.3}$$

$$u_q = R_s i_q + \frac{d\psi_q}{dt} + \omega_e \psi_d, \tag{2.4}$$

where:

- $u_d$ and $u_q$ are the d-axis and q-axis stator voltages, respectively.
- $R_s$ is the stator winding resistance.

- $i_d$ and $i_q$ are the d-axis and q-axis stator currents, respectively.
- $\psi_d$ and $\psi_q$ are the d-axis and q-axis stator flux linkages, respectively.
- $\omega_e$ is the electrical angular speed of the rotor.

The rotor voltage equation for the excitation winding is given by:

$$u_e = R_e i_e + \frac{d\psi_e}{dt}, \tag{2.5}$$

where:

- $u_e$ is the excitation voltage.
- $R_e$ is the rotor winding resistance.
- $i_e$ is the excitation current.
- $\psi_e$ is the excitation flux linkage.

### 2.0.4 Flux Linkage Equations

To ease the presentation of the proposed flux-weakening algorithm, linear current-to-flux linkage characteristics are assumed. The flux linkage equations in the dq reference frame are given by:

$$\psi_d = L_m i_e + L_d i_d \tag{2.6}$$

$$\psi_q = L_q i_q, \tag{2.7}$$

$$\psi_e = L_e i_e + \frac{3}{2} L_m i_d, \tag{2.8}$$

where:

- $L_d$ and $L_q$ are the d-axis and q-axis inductances, respectively.
- $L_e$ is the excitation inductance.
- $M_e$ is the mutual inductance between the stator d-axis and the rotor excitation winding.

### 2.0.5 Torque Equation

The torque produced by the EESM can be expressed in terms of the flux linkages and currents as:

$$T = \frac{3}{2}p(\psi_d i_q - \psi_q i_d), \tag{2.9}$$

Substituting the flux linkage equations (2.6) and (2.7) into the torque equation (2.9), we get:

$$T = \frac{3}{2}p\left[(L_m i_e + (L_d - L_q)i_d)i_q\right], \tag{2.10}$$

where:

- $T$ is the electromagnetic torque.
- $p$ is the number of pole pairs.

This torque equation shows that the torque is a function of both the stator and rotor currents as well as the flux linkages.

## 2.1 Base Point Calculation

Starting from the torque equation for an EESM:

$$T = \frac{3}{2}p\left[(L_m i_e + (L_d - L_q)i_d)\, i_q\right] \tag{2.11}$$

Substitute $i_q = I\sin(\alpha)$ and $i_d = I\cos(\alpha)$:

$$T = \frac{3}{2}p\left[(L_m i_e + (L_d - L_q)I\cos(\alpha))\, I\sin(\alpha)\right] \tag{2.12}$$

Simplify this expression:

$$T = \frac{3}{2}pI\sin(\alpha)\left[L_m i_e + (L_d - L_q)I\cos(\alpha)\right] \tag{2.13}$$

Let $I_N$ represent the magnitude of the stator current $I$:

$$T = \frac{3}{2}pI_N\sin(\alpha)\left[L_m i_e + I_N\cos(\alpha)(L_d - L_q)\right] \tag{2.14}$$

This is the desired torque equation:

$$T = \frac{3}{2}pI_N\sin(\alpha)\left(L_m i_e + I_N\cos(\alpha)(L_d - L_q)\right) \tag{2.15}$$

To find the optimal angle $\alpha$, we set the derivative of the torque with respect to $\alpha$ to zero:

$$\frac{dT}{d\alpha} = 0 \tag{2.16}$$

Taking the derivative of $T$ with respect to $\alpha$:

$$\frac{dT}{d\alpha} = \frac{3}{2} p I_N \left[ \cos(\alpha) \left( L_m i_e + I_N \cos(\alpha)(L_d - L_q) \right) - I_N \sin^2(\alpha)(L_d - L_q) \right] = 0 \tag{2.17}$$

Simplify and rearrange the equation:

$$\cos(\alpha) \left( L_m i_e + I_N \cos(\alpha)(L_d - L_q) \right) = I_N \sin^2(\alpha)(L_d - L_q) \tag{2.18}$$

Substitute $\sin^2(\alpha) = 1 - \cos^2(\alpha)$:

$$\cos(\alpha) \left( L_m i_e + I_N \cos(\alpha)(L_d - L_q) \right) = I_N (1 - \cos^2(\alpha))(L_d - L_q) \tag{2.19}$$

Rearrange the terms:

$$\cos(\alpha) L_m i_e + I_N \cos^2(\alpha)(L_d - L_q) = I_N (L_d - L_q) - I_N \cos^2(\alpha)(L_d - L_q) \tag{2.20}$$

Combine like terms:

$$\cos(\alpha) L_m i_e + 2 I_N \cos^2(\alpha)(L_d - L_q) = I_N (L_d - L_q) \tag{2.21}$$

Let $x = \cos(\alpha)$:

$$x L_m i_e + 2 I_N x^2 (L_d - L_q) = I_N (L_d - L_q) \tag{2.22}$$

Rearrange into a quadratic equation:

$$2 I_N (L_d - L_q) x^2 + L_m i_e x - I_N (L_d - L_q) = 0 \tag{2.23}$$

Solve the quadratic equation for $x$:

$$x = \frac{-L_m i_e \pm \sqrt{(L_m i_e)^2 + 8 (L_d - L_q)^2 I_N^2}}{4 (L_d - L_q) I_N} \tag{2.24}$$

Therefore,

$$\cos(\alpha) = \frac{-L_m i_e + \sqrt{(L_m i_e)^2 + 8(L_d - L_q)^2 I_N^2}}{4(L_d - L_q) I_N} \tag{2.25}$$

Thus, the optimal angle $\alpha$ is:

$$\alpha = \arccos\left(\frac{-L_m i_e + \sqrt{(L_m i_e)^2 + 8(L_d - L_q)^2 I_N^2}}{4(L_d - L_q) I_N}\right) \tag{2.26}$$

By solving the torque optimization equations, we obtain the following results for the motor parameters: the optimal angle $\alpha = 62.47°$, the direct-axis current $I_d = 340.2\,\text{A}$, the quadrature-axis current $I_q = 652.66\,\text{A}$, the maximum torque at base speed $\tau = 1177\,\text{N}\cdot\text{m}$, and the base speed $W_B = \frac{V_N}{\sqrt{(L_d I_d + L_m I_e)^2 + (L_q I_q)^2}} = 1570\,\text{rad/s}$.

By solving the torque optimization equations, we obtain the following results for the motor parameters:

- Optimal angle: $\alpha = 62.47°$
- Direct-axis current: $I_d = 340.2\,\text{A}$
- Quadrature-axis current: $I_q = 652.66\,\text{A}$
- Maximum torque at base speed: $\tau = 1177\,\text{N}\cdot\text{m}$
- Base speed:

$$W_B = \frac{V_N}{\sqrt{(L_d I_d + L_m I_e)^2 + (L_q I_q)^2}} = 1560\,\text{rad/s}$$

These numbers indicate the EESM's best performance variables for the specified working condition. The optimum $\alpha$ angle ensures quick achievement of maximum torque, while direct and quadrature axis currents are responsible for this optimal work rate. The calculation of the base speed shows that at the rated voltage $V_N$, the motor has a base speed of 1560 rad/s.

In figure 3 above, it depicts the limit circle and motor operating limits curves, and also shows the nominal torque curve with ellipse at base speed.

### 2.1.1 Summary

The aforementioned equations present an inclusive mathematical model of EESM in rotating dq reference frame. This model provides a starting point for control strategies development such as Maximum Torque per Ampere (MTPA), flux weakening, and Maximum Torque per Voltage (MTPV) which will be highlighted on later chapters. By assuming linear current-to-flux linkage characteristics in this case, these control algorithms can be easily analysed and designed.

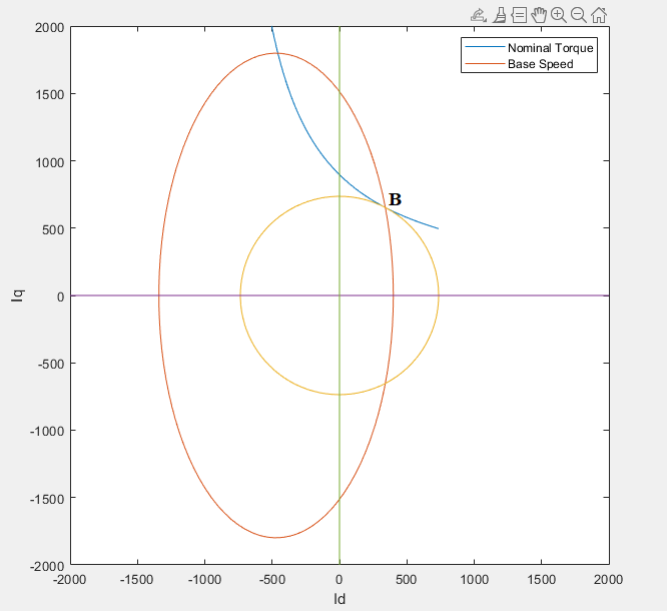


Figure 2.3: The $(i_d, i_q)$ plane representing current and voltage constraints

## 2.2 MTPA, FLux Weakening, and MTPV Control Startegies

In this part, we will discuss the methods of controlling the weakening of flux in EESM. We will focus on the Maximum Torque Per Ampere (MTPA), flux weakening, and Maximum Torque Per Voltage (MTPV) strategies. These are techniques that have been implemented to expand the field of operation of the motor while ensuring that it remains highly effective under different speed and load conditions.

### 2.2.1 Current and Voltage Constraints for EESM

Real applications have some constraints to prevent damages or failures. The minimum value of maximum for each component must be chosen as the maximum magnitude of current and voltage that system can handle. To maintain these within their limits, following restrictions should apply:

$$[h]i_d^2 + i_q^2 \leq I_{s,\max}^2 \tag{2.1}$$

$$v_d^2 + v_q^2 \leq V_{s,\max}^2 \tag{2.2}$$

This section examines previously introduced constraints and provides a limit in $(i_d, i_q)$ coordinates. In order to graphically illustrate this restriction with a plane, here is an example:

The first limit, that is expressed by equation (2.1), makes the current vector magnitude to be

lower than the maximum nominal current. Graphically, it consists of a circle centered at $(0, 0)$ in the $(i_d, i_q)$ plane with a radius equal to $I_{s,\max}$. This bound will be called the circle limitation.

Taking into account the voltage limitation expressed by equation (2.2), we can re-manage the bound relation to describe an allowable current area in the $(i_d, i_q)$ plane. Neglecting the voltage drop due to the current that flows through the stator resistance $R_s$, the limitation can be rewritten as follows:

$$L_d \left( \frac{L_m i_e}{L_d} + i_d \right)^2 + L_q^2 i_q^2 \leq \left( \frac{V_{s,\max}}{\omega_m} \right)^2 \tag{2.3}$$

Thus, the allowable region for voltage restriction is represented by an ellipse centred at $\left(-\frac{L_m i_e}{L_d}, 0\right)$.This kind of current limit will be referred to as a voltage ellipse bound. The permissible points of operation are all $(i_d, i_q)$ pairs lying inside the region described by the voltage ellipse and current circle..

### 2.2.2 Current Trajectory

t is very important to define what makes up an admissible control area in terms of $(i_d, i_q)$ so that the motor can work properly within its own current and voltage limits. Once this area has been set up, different classical control techniques could then be employed with a view to optimizing motor performance regarding current consumption, torque production, and speed [9].

One such widely used technique is the Maximum Torque Per Ampere (MTPA) control strategy. It aims to minimize the current that is required to generate the reference torque. By identifying the optimum $(i_d, i_q)$ trajectory, MTPA guarantees the best performance with reduced iron losses. The MTPA trajectory holds true up till base speed, $\omega_{rb}$. beyond which flux magnitude must be decreased in order to achieve higher speeds [15].

In addition to MTPA, another important strategy is Maximum Torque Per Voltage (MTPV) trajectory. This method becomes necessary at higher speeds where it is crucial to reduce the current amplitude to stay within the voltage limits of the motor. This region is known as the voltage-limited region.

The current trajectory can be divided into distinct segments:

- **OA:** Represents the MTPA trajectory where the motor operates efficiently by minimizing current consumption.
- **AB:** Denotes the flux weakening with a constant current trajectory, allowing the motor to achieve speeds higher than the base speed.
- **BC:** Corresponds to the Maximum Torque Per Voltage (MTPV) trajectory, essential for maintaining torque output while respecting voltage constraints at high speeds.

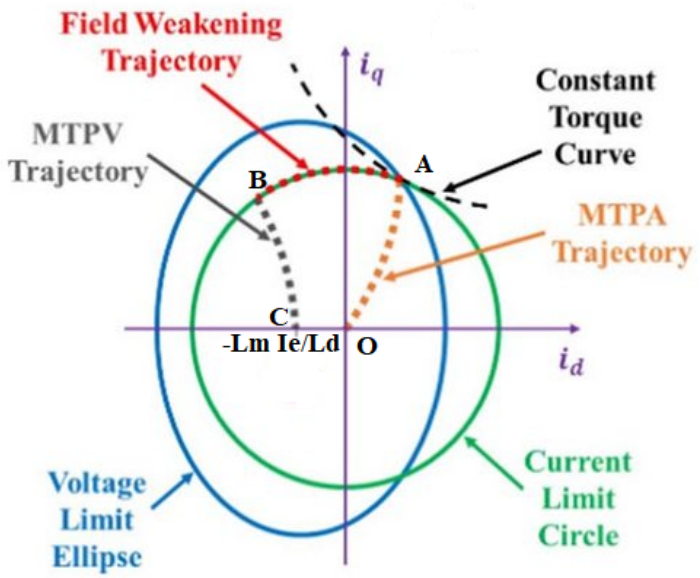


Figure 2.4: Typical $(i_d, i_q)$ current trajectory for IPM motors.

These control strategies are essential for optimizing the performance of EESM motors, ensuring they operate within safe electrical limits while delivering the required torque and speed characteristics.

### 2.2.3 MTPA Trajectory

the torque equation of an EESM in the $d$–$q$ reference frame can be expressed as:

$$T_e = n_p \left[ (L_d - L_q) i_d i_q + L_m i_e i_q \right] \tag{2.27}$$

As described by Equation 27, we can obtain the same amount of torque with different combinations of $i_d$ and $i_q$. It is possible to express a current vector in the $d$–$q$ reference frame by using its magnitude and the angle described by the vector itself and the real axis:

$$\begin{cases} i_d = I_N \sin \beta \\ i_q = I_N \cos \beta \end{cases} \tag{2.28}$$

Then as explained above the base point can be found with the specified Id and Iq value which are 340 A and 652 A respectively.

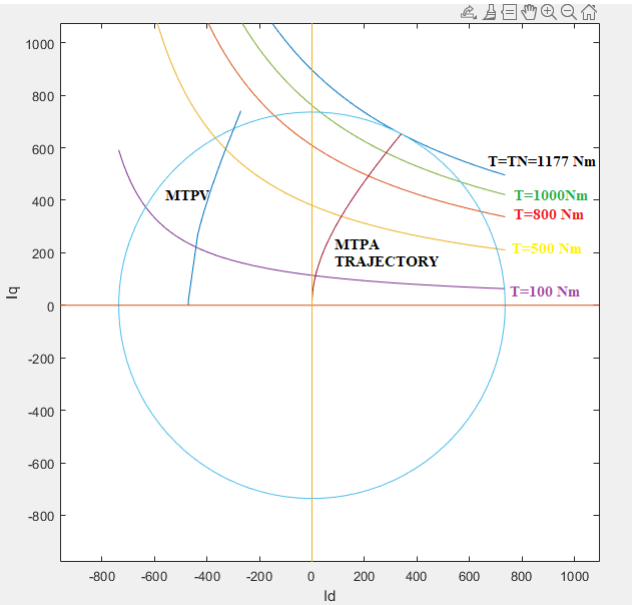


Figure 2.5: Limit Circle Diagram exhibiting Torque curve with MTPA Trajectory

### 2.2.4 Flux Weakening Trajectory

The previous strategy is suitable up to the base speed, $\omega_b$, in motor coordinates. At base speed, the terminal voltage of the motor reaches its maximum value. To increase the motor speed beyond this point, a control strategy to reduce the stator flux must be implemented. By applying a demagnetizing magnetomotive force (MMF) through the manipulation of stator currents, the effective MMF generated can be reduced, allowing the motor speed to increase. This strategy is known as field-weakening (FW). This transition occurs at point A in Figure 4, where the BackEMF force equals the maximum voltage that can be supplied to the motor.

$$V_{\text{max}} = \omega_b |\psi_{\text{tot}}| \tag{2.29}$$

When $\omega_m$ is greater than $\omega_b$, the maximum $|\psi_{\text{tot}}|$ allowed is:

$$|\psi_{\text{tot}}| = \frac{V_{\text{max}}}{\omega_b} \tag{2.30}$$

To achieve a smaller flux magnitude, a common strategy is to increase the $\beta$ current angle. By increasing the current angle, the demagnetizing component, which is opposite to the flux component $L_m i_e$, becomes larger, thereby reducing the overall flux amplitude. This behavior is evident from the flux components in the motor model equations:

$$\begin{cases} \psi_d = L_d i_d + L_m i_e \\ \psi_q = L_q i_q \end{cases} \tag{2.31}$$

This set of equations is also known as the magnetic model. A typical flux weakening trajectory for an EESM is the AB arc in Figure 4.

Additionally, high operating speeds can be managed through the following derived equation:

$$\left(\frac{V_N}{\omega}\right)^2 = (L_m i_e + L_d I_N \cos\alpha)^2 + (L_q I_N \sin\alpha)^2 \tag{2.32}$$

Expanding and solving for $\alpha$:

$$(\cos\alpha)^2 \left((L_d I_N)^2 - (L_q I_N)^2\right) + 2L_m i_e L_d I_N \cos\alpha + (L_q I_N)^2 + (L_m i_e)^2 - \left(\frac{V_N}{\omega}\right)^2 = 0 \tag{2.33}$$

By solving this equation, we can determine the optimal $\alpha$, $i_d$, and $i_q$ values for flux weakening, ensuring that the motor operates efficiently at high speeds while maintaining the desired performance.

### 2.2.5 Maximum Torque Per Voltage (MTPV)

The Maximum Torque Per Voltage (MTPV) operation takes place at very high speeds in the field-weakening (FW) area of an EESM motor. In this area, the major constraint becomes voltage limit. After reaching a certain speed point, max torque is no longer achievable by utilizing full inverter current. At this point, the current references must be derived based on the tangential intersection between the torque curves and the shrinking voltage ellipses [16].

To derive the MTPV currents for an EESM motor, we start with looking at voltage equation under field-weakening (FW) operation. Equation for voltage in terms of flux linkages is:

$$\left(\frac{V}{\omega}\right)^2 = \lambda_d^2 + \lambda_q^2$$

where $\lambda_d = L_m I_e + L_d I_d$ and $\lambda_q = L_q I_q$.

Substituting $\lambda_d$ and $\lambda_q$ into the voltage equation, we get:

$$\left(\frac{V}{\omega}\right)^2 = (L_m I_e + L_d I_d)^2 + (L_q I_q)^2$$

To simplify the analysis, we introduce a new current term $I_{dch}$ such that $L_m I_e + L_d I_d = L_q I_{dch}$. Substituting this into the voltage equation, we have:

$$\left(\frac{V}{\omega}\right)^2 = (L_q I_{dch})^2 + (L_q I_q)^2$$

Rewriting, we obtain:

$$\left(\frac{V}{\omega L_q}\right)^2 = I_{dch}^2 + I_q^2$$

This represents a new limit circle in the $I_q$ and $I_{dch}$ plane with a radius of $\frac{V}{\omega L_q}$. Here, $I_{dch}$ is given by:

$$I_{dch} = \frac{L_m I_e + L_d I_d}{L_q}$$

Next, we consider the torque equation:

$$T = \frac{3}{2} p \left[ L_m I_e I_q + (L_d - L_q) I_d I_q \right]$$

Substituting $I_d$ in terms of $I_{dch}$, where $I_d = \frac{L_q I_{dch} - L_m I_e}{L_d}$, the torque equation becomes:

$$T = \frac{3}{2} p \left[ L_m I_e I_q + (L_d - L_q) \left( \frac{L_q I_{dch} - L_m I_e}{L_d} \right) I_q \right]$$

Simplifying, we get:

$$T = \frac{3}{2} p \left( \frac{L_q}{L_d} \right) \left[ L_m I_e + (L_d - L_q) I_{dch} \right] I_q$$

Given the new limit circle, we know:

$$I_{dch} = \frac{V}{\omega L_q} \cos\beta \quad \text{and} \quad I_q = \frac{V}{\omega L_q} \sin\beta$$

Substituting these into the torque equation, we have:

$$T = \frac{3}{2} p \left( \frac{L_q}{L_d} \right) \left[ L_m I_e + (L_d - L_q) \left( \frac{V}{\omega L_q} \cos\beta \right) \right] \left( \frac{V}{\omega L_q} \sin\beta \right)$$

To find the optimal angle $\beta$, we solve for $\frac{dT}{d\beta} = 0$:

$$\frac{dT}{d\beta} = \frac{3}{2} p \left( \frac{L_q}{L_d} \right) \left( \frac{V}{\omega L_q} \right)^2 \left[ L_m I_e \cos\beta + (L_d - L_q) \left( \cos^2\beta - \sin^2\beta \right) \right]$$

Setting this to zero:

$$L_m I_e \cos\beta + (L_d - L_q) \left( \cos^2\beta - \sin^2\beta \right) = 0$$

Simplifying and solving for $\cos\beta$, we get:

$$\cos\beta = \frac{-L_m I_e \pm \sqrt{(L_m I_e)^2 + 8(L_d - L_q)^2 \left(\frac{V}{\omega L_q}\right)^2}}{4(L_d - L_q)\left(\frac{V}{\omega L_q}\right)}$$

With $\cos\beta$ known, we can determine $\beta$ and subsequently $I_{dch}$ and $I_q$:

$$I_{dch} = \frac{V}{\omega L_q}\cos\beta$$

$$I_q = \frac{V}{\omega L_q}\sin\beta$$

Finally, $I_d$ can be found using $I_{dch}$:

$$I_d = \frac{L_q I_{dch} - L_m I_e}{L_d}$$

Thus, $I_d$ and $I_q$ produced through these steps are actually MTPV currents for EESM motor. This ensures that optimal performance is achieved under voltage constraint at high speeds.

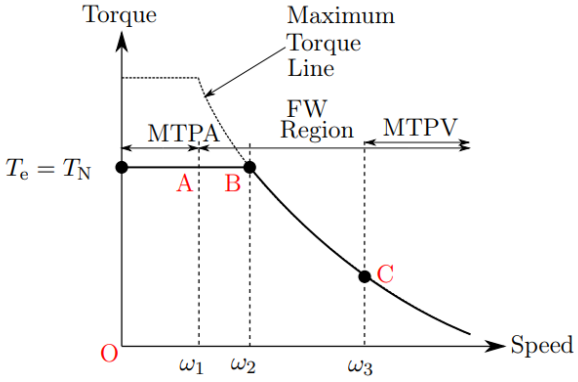


Figure 2.6: Torque Vs Speed Characteristics

The torque-speed curve of an EESM motor can be divided into three distinct regions: Maximum Torque Per Ampere (MTPA) region, Field-Weakening (FW) region, and Maximum Torque Per Voltage (MTPV) region. These regions use different control strategies to maximize motor performance under varying speed conditions.

MTPA region is a torque-speed area in which the motor runs at its maximum available torque by optimizing the current in windings of stator. This area is defined from A to B on the torque-speed curve. In so doing, the control scheme for maintaining this condition makes sure that the motor produces maximum torque per unit of current by suitably manipulating id and iq currents.

While speed increases up to base speed $\omega_B$, the torque remains constant but it is at its highest

value. MTPA control ensures that minimum possible current draw is achieved by aligning the current vector while maximizing torques output.

Beyond base speed $\omega_B$, FW region starts indicated by line segment BC on the torque –speed curve. Here, further increase in speed can only be obtained through reducing stator flux as indicated by an upper limit established for terminal voltage.

The FW control strategy entails changing stator currents so that a de-magnetizing magnetomotive force (MMF) arises. This results into reduced flux linkage that occurs within a motor enabling it to reach higher speeds; however it leads to lower torque as rotational velocity goes up.

Both current and voltage limitations are highly influential in curtailing any rise of the torques during FW operating modes. The voltage ellipse shrinks as the speed increases, pushing the operating point towards the center.

At very high speeds, the motor works in the MTPV region, after point C on the torque-speed curve. In this region, achieving maximum torque is limited by the available voltage and current. The MTPV control strategy gets the current references from where the torque curves intersect and cross tangentially with shrinking voltage ellipses.

The torque continues to decrease while the speed increases in the MTPV region. The solution of the current limit and voltage limit equations gives the optimal current references for this region. The objective here is to maximize the speed while keeping the torque within limits of voltage and current that the motor can handle.

The graph above depicts the transition through these areas, as speeds increases past base speed and torque falls. The above attribute is intrinsic to high-speed EESM motors since a variety of control strategies are used to better the performance for various operating scenarios.

## 2.3 Speed Control of EESM Linear Model

This part explains the speed control method of Externally Excited Synchronous Machines (EESMs) that is almost the same as that of Interior Permanent Magnet (IPM) machines. The control architecture of the vehicle uses a PI controller for speed regulation, and current controls blocks and other higher function blocks such as MTPA (Maximum Torque per Ampere), FW (Field Weakening), and MPTV (Maximum torque per voltage).

Figure **??** illustrates the overall block diagram of the speed control system for EESM.

The overall control system operates as follows:

1. **Speed PI Controller:** The desired speed ($\omega_{ref}$) is compared with the actual speed ($\omega$) of the motor. The error is processed by a Proportional-Integral (PI) controller to generate a torque reference ($T_{ref}$).

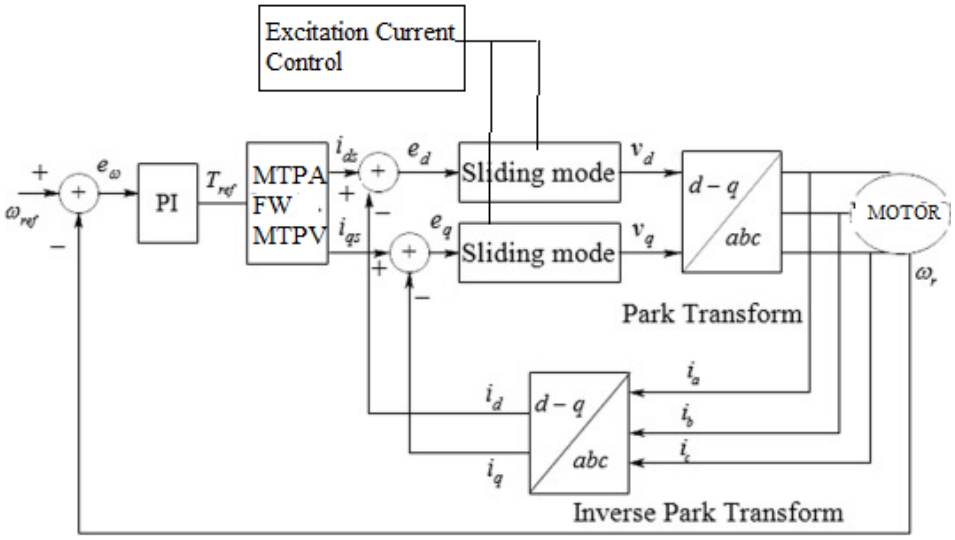


Figure 2.7: Speed Control Block Diagram

2. **MTPA/FW/MTPV Control Block:** The torque reference is fed into a control block that selects the appropriate strategy based on the operating region. As mentioned in the sections above, the MTPA strategy is used for low-speed operation to maximize torque per ampere. As the speed increases, the system transitions to the FW region to extend the speed range by weakening the magnetic field. At very high speeds, the MTPV strategy ensures optimal torque output within voltage limits.

3. **Current Control Block:** The selected strategy determines the reference currents ($i_{d,ref}$ and $i_{q,ref}$), which are then regulated by the current control block. This block typically includes PI controllers for both $i_d$ and $i_q$, ensuring that the motor currents follow their respective reference values accurately.

This overall block diagram illustrates the high-level view of the speed control strategy applied for EESM. Each component—current control blocks, speed PI controller, and MTPA/FW/MTPV control block—has a very important role in ensuring that it achieves the best possible motor performance within this wide range of variation in operating conditions.

In the following sections of the thesis, we will look at each of these components in great detail. We will first of all look in detail at the current methodology in place, discussing specifically how d-axis current and q-axis current controllers have been developed and integrated into their respective controls. We will then examine the speed PI control with even greater resolution, considering its tuning and characteristics. To complete this aspect of the description, we will also present in detail the MTPA, FW, and MTPV control strategies and how all of these can be dovetailed into an overall speed control system to significantly improve EESM performance.

## 2.4 Current Control

In control of electric machines, especially for the EESM motor, large dependence on the level of d-axis and q-axis currents is placed in order to realize its optimum operation. Usually, the d–axis current, $i_d$, controls the magnetic flux in the machine, with the q–axis current, $i_q$, responsible for the torque production. With independent control of these currents, it should be possible to ensure optimum performance of the motor under various operating conditions.

For instance, in the MTPA operational strategy, the currents are controlled by enabling the torque efficiency in lower speed operations. The $i_d$ component is increased in the FW operating region to reduce flux linkage for higher speeds than base speed while managing voltage constraints. Finally, in the Maximum Torque Per Voltage region, the current references are adjusted to perfectly balance voltage and current limits at very high speeds for optimized torque output. This independent control of $i_d$ and $i_q$ currents is basic to more advanced techniques of motor control and gives flexibility in enhancing efficiency, extending the speed range, and improving overall performance of motors.

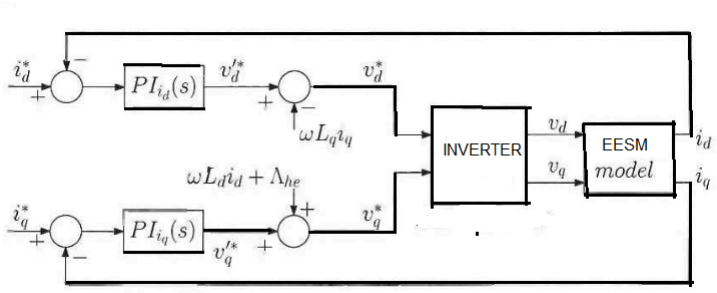


Figure 2.8: Current Control Loops

The control strategy is founded on an advanced block diagram, which starts with the transformation of three-phase stator currents $(i_a, i_b, i_c)$ in the $d$-$q$ frame of reference using both Clarke and Park transformations. In this context, the decoupled current control is performed, including distinct PI controllers for $i_d$ and $i_q$, duly endowed with suitable compensation mechanisms against the given dynamics and cross-coupling effects. These controllers generate voltage commands $V_{d,\text{ref}}$ and $V_{q,\text{ref}}$ based on the error between reference currents $i_{d,\text{ref}}$, $i_{q,\text{ref}}$ and their actual counterparts $i_d$, $i_q$. The following Inverse Park Transformation converts these commands back to the stationary reference frame. Then, Space Vector Pulse Width Modulation (SVPWM) is done to get the required three-phase voltage vectors for the inverter.

The inverter, modulated by SVPWM signals, converts the DC voltage from a supply into an AC voltage that will provide the required accuracy to drive a motor. This action by the motor, due to the applied $V_d$ and $V_q$ voltages, allows the desired current values of $i_d$ and $i_q$ to reach their respective setpoints, thus ensuring the best torque and flux control within the whole operational

range of the motor. This structured approach ensures efficient performance across a wide range of varying operational conditions, therefore greatly contributing to enhanced motor efficiency, extended speed range, and overall system reliability.

### 2.4.1 PI Controller Design Using Bode Method for Current Control

High accuracy current control in electric machine drive systems is critically required to ensure overall performance under various operating conditions. This subsection looks into the design of Proportional-Integral controllers by the Bode method to ensure robust stability and current regulation performance in EESMs.

#### System Model and Block Diagram

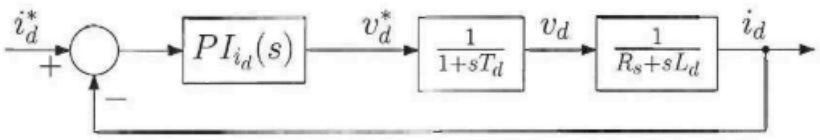


Figure 2.9: Simplified Current Control Loop

Consider the simplified block diagram of an electric motor system, where the armature impedance is modeled as $\frac{1}{R+Ls}$, with $R$ denoting resistance and $L$ representing inductance. A PI controller has to keep the d-axis current $i_d$ and the q-axis current $i_q$ by their reference values $i_{d,ref}$ and $i_{q,ref}$. The voltage commands $V_{d,ref}$ and $V_{q,ref}$ from the PI controller are further processed by an inverter block represented by $\frac{1}{Ts+1}$, which models the average delay introduced by the inverter.

#### Bode Analysis for PI Controller Design

The Bode method is a systematic design approach for the PI controllers of a problem by investigating the frequency response of the closed-loop system. The methodology is supported by the following steps:

1. **Open-Loop Transfer Function:**

   Derive the open-loop transfer function $L(s)$ of the system:

$$L(s) = K_i \cdot \frac{1 + sT_{pi}}{s} \cdot K_c \cdot \frac{1 + sT_c}{1} \cdot \frac{1}{R} \cdot \frac{1}{1 + sT_e}$$

Here, $K_i$ is the integral gain, $T_{pi}$ is the PI controller time constant, $K_c$ is the proportional gain, $T_c$ is the current controller time constant, $R$ is the resistance, and $T_e$ is the electrical time constant.

2. **Phase Margin Calculation:**

   The desired phase margin is determined by setting:

$$\angle L(j\omega_B) = -180^\circ + \phi_m = -110^\circ$$

   This implies:

$$\arctan(\omega_B T_{pi}) - 90^\circ - \arctan\left(\frac{\omega_B}{\omega_{n1}}\right) - \arctan\left(\frac{\omega_B}{\omega_{n2}}\right) = -110^\circ$$

   Solving for $T_{pi}$ yields a general form without specific values. The time constant $T_{pi}$ ensures the required phase margin.

3. **Gain Adjustment:**

   To achieve unity gain at the crossover frequency $\omega = \omega_B$:

$$|L(j\omega_B)| = K_i \cdot \sqrt{\frac{1}{1+(\omega_B T_{pi})^2}} \cdot \omega_B \cdot \sqrt{\frac{\omega_{n1}}{1+\left(\frac{\omega_B}{\omega_{n1}}\right)^2}} \cdot \sqrt{\frac{1}{1+\left(\frac{\omega_B}{\omega_{n2}}\right)^2}} = 1$$

   Solving for $K_i$ in general form ensures unity gain at the desired crossover frequency. Given $T_{pi} = \frac{K_p}{K_i}$, solving for $K_p$ provides the proportional gain required for the desired phase margin and gain crossover frequency.

Listing 2.1: PI calculations

```
Pd=(1/(1+s*Td))*(1/(R+s*Ld));
Pq=1/((1+s*Td)*(R+s*Lq));
[Kpd, Kid, Tpid] = pid_bode(Pd,3000,70*deg2rad);
[Kpq, Kiq, Tpiq] = pid_bode(Pq,3000,70*deg2rad);
function [Kp, Ki, Tpi] = pid_bode(P1,wgc,phasemrgn)
Pcmplx=evalfr(P1,1i*wgc);
Tpi=(tan(-pi+phasemrgn-angle(Pcmplx)+pi/2))/wgc;
Ki = (1/abs(Pcmplx))*(wgc/sqrt(1+(wgc*Tpi)^2));
Kp = Ki*Tpi;
end
```

The PI controller gains were implemented and tuned with this function pid-bode in which it takes the plant, cross over frequency, and the desired phase margin as an input and return the gains values. here for this motor it has been found that Kid= 197.7, Kpd=0.968, Kiq=111.169 and Kpq=0.4685.

Then using this method after choosing the crossover frequency of about 3000 rad/s and phase margin of 70 degrees, here in the next figure shows the bode plot of the open loop control along the d and q axis.

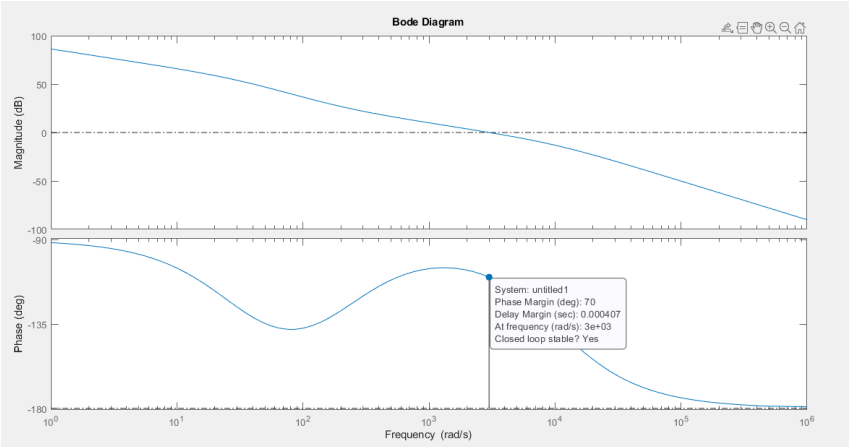


(a) Id Bode Plot

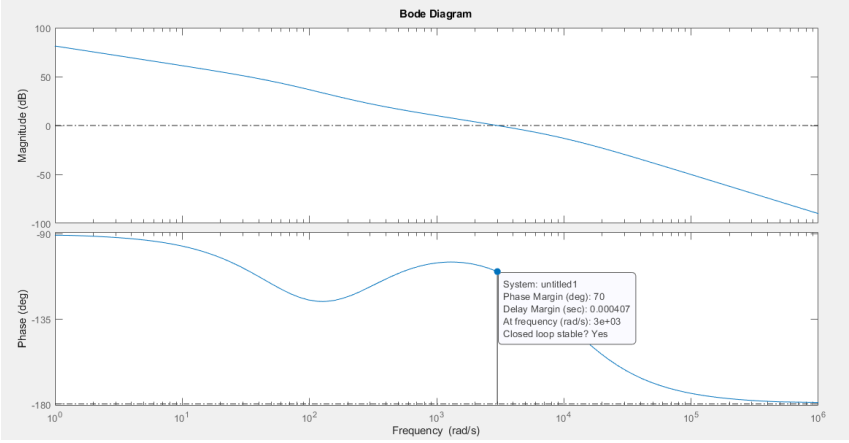


(b) Iq Bode Plot

Figure 2.10: Bode Plot of open loop control along d and q axis.

as seen in the bode plot here the phase margin is 70 degrees and the crossing at 3700 rad/sec happens with a -20 dB/dec which implies that the system is stable. Here in the figure below, I will show the transient response of the designed controllers.

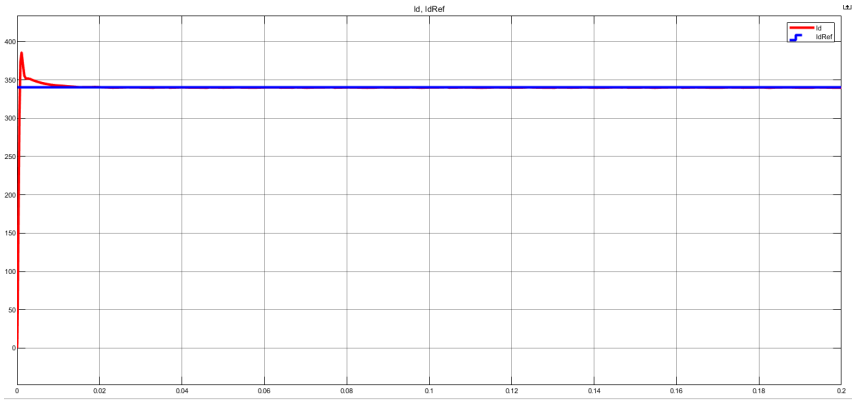


(a) Id

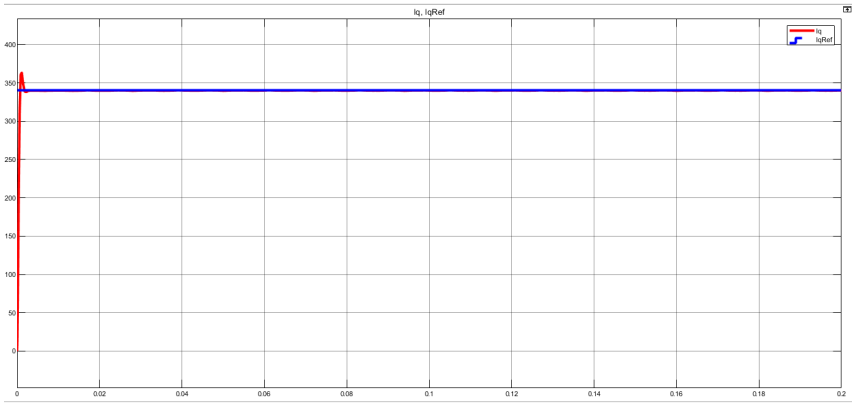


(b) Iq

Figure 2.11: Transient Response of both Current Controllers.

As shown in figure the transient response here shows a very fast-tracking of the step of 340 amps for both Id and Iq, which is very important for our control.

### 2.4.2 Anti-Windup Addition

In general, anti-windup methodologies have significantly enhanced the overall response of the control system. Anti-windup mechanisms played a very vital role in the taming of integrator windup problems that usually impaired the performance of feedback controllers. Dealing effectively with integrator saturation during operation ensured smoother transitions and quicker recovery times, hence improving the transient response and stability of a system. The anti-windup application handled not only the constraints coming from actuator limits but also achieved optimization of the controller in terms of disturbance rejection and set-point tracking with better desired values. In this regard, extensive experiments, complemented by analysis, showed that a great deal of system performance improvement had been enhanced by anti-windup strategies for enhancing the overall response and robustness of a control system. Anti-windup was an

important aspect that had to be taken into consideration in this model. Simulation results with and without the anti-windup will be discussed in the next section.

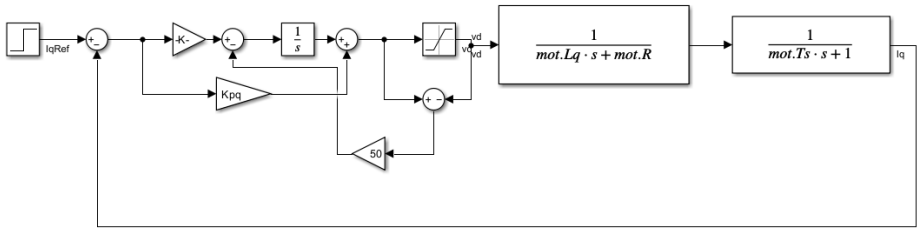


Figure 2.12: Simulink I control Loop with Anti-windup

## 2.5 Simulink Modelling

As illustrated in Figure 13, the Simulink model of the speed control for the linear model of the motor is exploited. As mentioned, it is going to be divided into three principle parts: the speed control block, then the MTPA, and, finally, the Flux weakening/MTPV block that calculates the Id and Iq reference signals depending on the reference speed and the control signal coming from the speed control. This will be followed by the current control blocks Id, Iq, and Ie, and finally, the dynamic model of the motor simulation. The objective is to optimize the motor performance across different operating conditions.

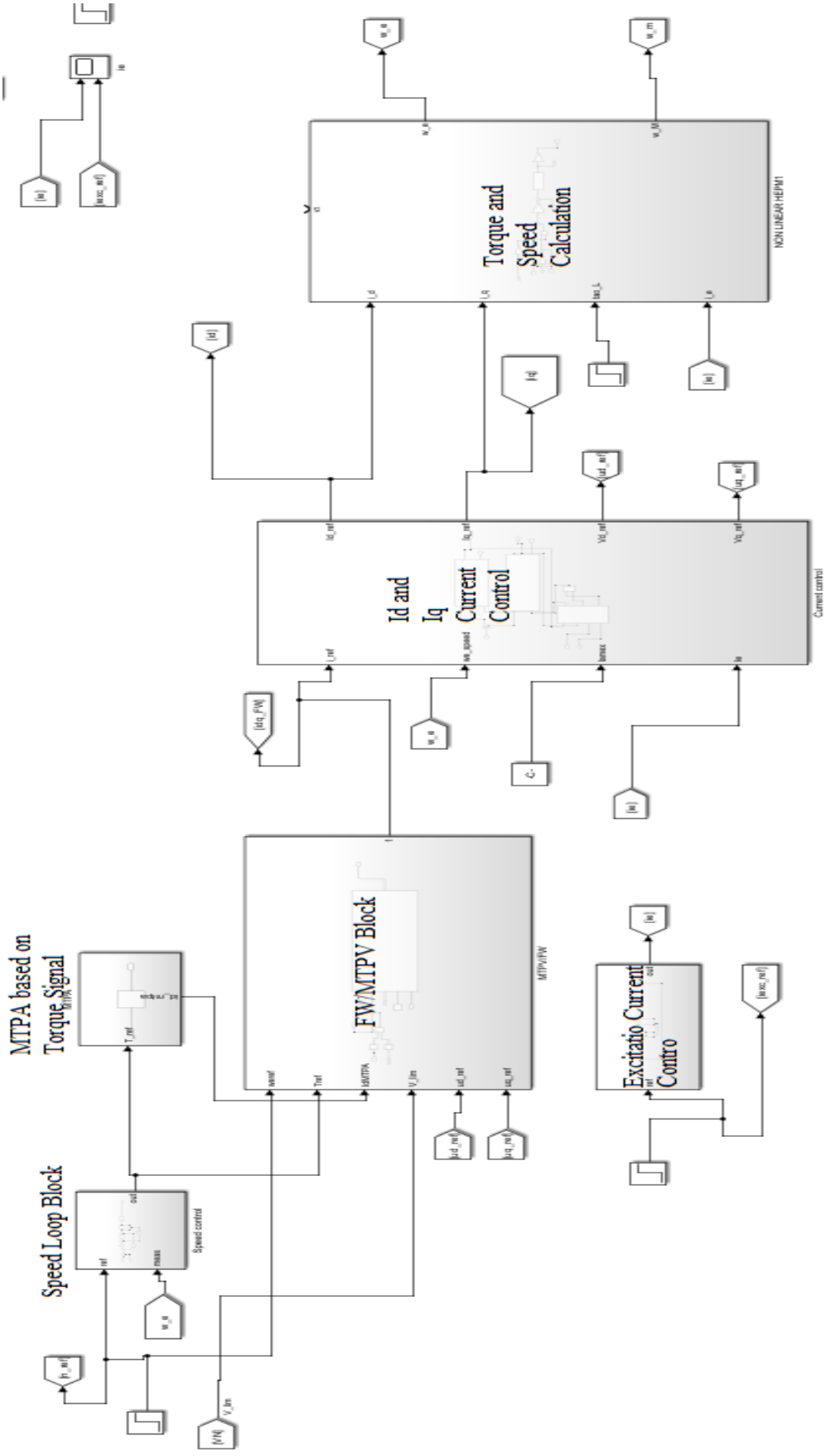


Figure 2.13: Simulink Model of Speed Control of the Linear model of the Motor

The Simulink model is composed of several interconnected blocks and subsystems, each responsible for a specific aspect of the motor control. The primary components include:

- Speed control block with a PID controller
- Lookup table for IdMTPA calculation
- FW/MTPV block for high-speed operations
- Current control blocks with PI controllers and compensation mechanisms
- Torque calculation block
- Speed calculation block incorporating dynamics such as friction and moment of inertia

### 2.5.1 Speed Control Block

The speed control block utilizes a PI controller with anti-windup, which generates the reference torque, $T_{ref}$. Anti-windup prevents chattering and integral windup, which significantly improves the transient response of the system. The PID controller evaluates $T_{ref}$ from an error formed between the speed command, $\omega_{ref}$, and the actual speed, $\omega$. The PI controller gains

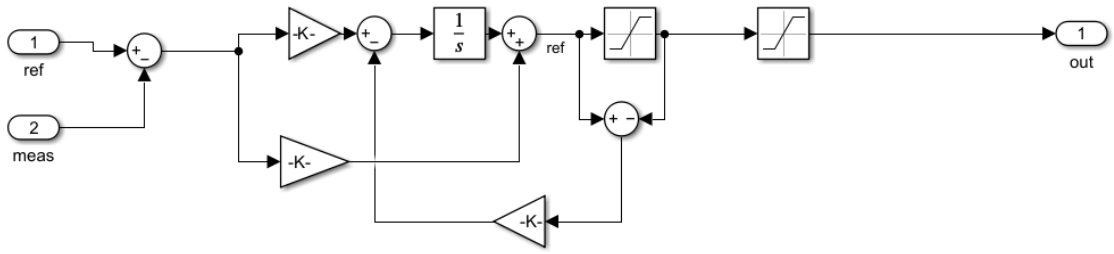


Figure 2.14: Speed control Loop

were tuned using the PID function illustrated previously, the output control signal is considered to be the reference torque that will have a crucial role in calculating the reference currents. The reference torque ($T_{ref}$) is computed as:

$$T_{ref} = K_p e(t) + K_i \int e(t)\, dt \tag{2.34}$$

where $e(t) = \omega_{ref} - \omega$ is the speed error. and of course the torque is limited with the maximum torque value of 1177 Nm.

**Anti-wind up**

Anti-windup is one of the most important techniques in motor speed control, particularly with PI controllers. Usually, in speed control, the integral part of the PI controller will continue to build up a large error when the actuator, which refers to the motor here, has been saturated and cannot follow the control signal. This can result in overshoot and long settling times when the actuator is no longer saturated; this is known as "integral windup." Anti-windup mechanisms prevent the accumulations of error by the integrator during periods of saturation, ensuring response to set-point or load changes is much faster and more accurate. On the note of saturation, anti-windup limits the integrator output, hence ensuring a very high level of stability of the system with less overshoot, which confirms that the given speed control system is suitable to achieve effective and reliable operation of a motor. It could be implemented with the following anti-windup

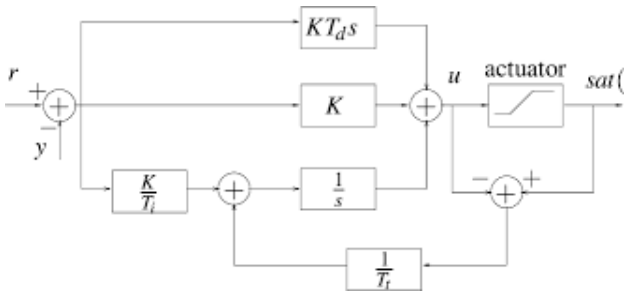


Figure 2.15: Possible Implementation of Anti-windup

### 2.5.2 MTPA and FW/MTPV Blocks

After the reference Torque is calculated, the next step is to use the LUT that has been found to implement the MTPA trajectory. In which the current follows this trajectory when the speed is below the base speed. To implement this trajectory on Matlab the data of the trajectory was taken on an external code and then was put in this Look-up table so the Id MTPA value is the output of this block.

The following table represents the Lookup Table (LUT) for Maximum Torque Per Ampere (MTPA). This table maps the d-axis current (Id) to the corresponding torque values. Then after finding the MTPA current we have to decide on what region of the circle we are on, so for values less than the calculated base speed only MTPA trajectory will be used, if it on high speed we have to decrease the flux by moving the current vector to the left up to certain point, then we have to move to MTPV trajectory. This is implemented in a way that will be explained here in the coming figures.

| Id (A) | Torque (Nm) |
|---|---|
| 0 | 0 |
| 0.31 | 20 |
| 6.28 | 100 |
| 23.6 | 200 |
| 48.95 | 300 |
| 79.24 | 400 |
| 112.2 | 500 |
| 146.5 | 600 |
| 181.0 | 700 |
| 248.4 | 900 |
| 282.2 | 1000 |
| 340.2 | 1177 |

Table 2.1: MTPA Lookup Table

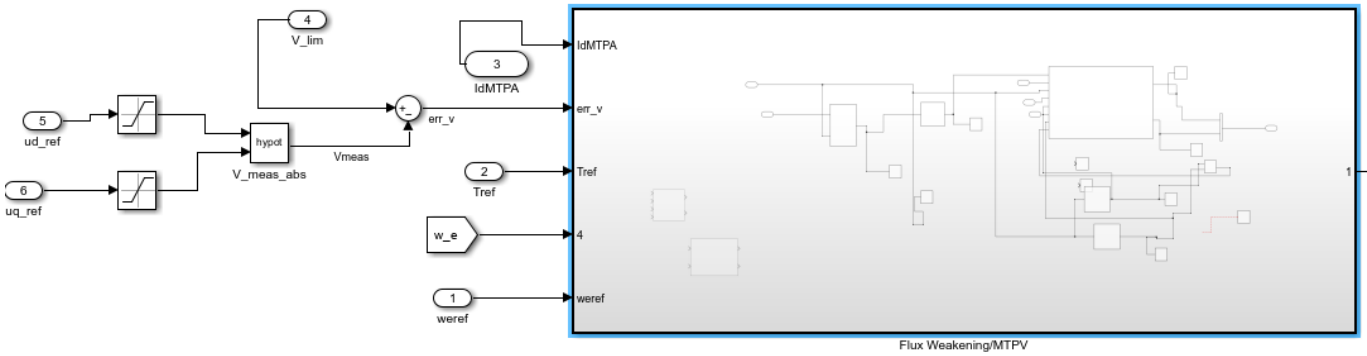


(a) FLux Weakening Block

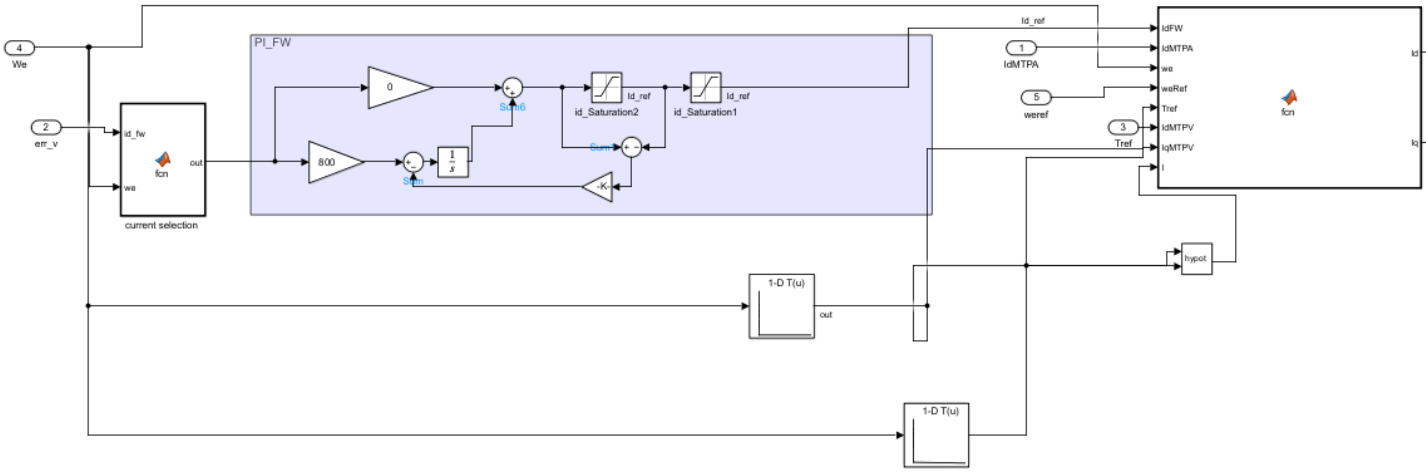


(b) Flux Weakening Block from inside



Figure 2.16: FW/MTPV Block

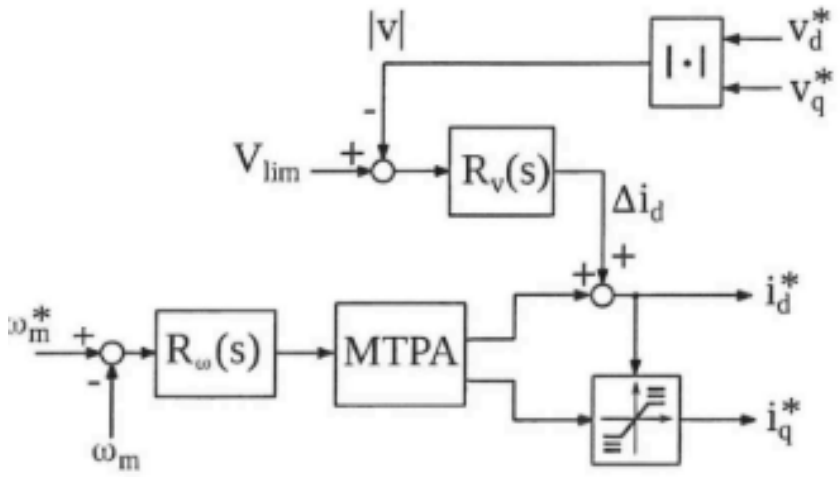


Figure 2.17: FLux Weakening Technique Implemented

Voltage reference ($V_{ref}$) are used instead of actual motor terminal voltages. These references determine the amplitude $|v|$ of the voltage vector required at the motor's operating point. The reference $|v|$ is compared to a voltage limit $V_{lim}$. If $|v| > V_{lim}$, the Flux Weakening (FW) block intervenes.

The FW block modifies the components of the current space vector based on inputs from the Maximum Torque Per Ampere (MTPA) block. It adjusts the current components if a voltage higher than $V_{lim}$ is necessary.

The applied voltage to the motor is constrained by the DC-link voltage ($V_N$). Therefore, the voltage references from current regulators are also limited. The voltage loop activates only when $V_{ref} > V_{lim}$, ensuring $V_{lim}$ is less than $V_N$ to control the stator voltage effectively (typically $V_{lim} = 0.9V_N$).

The voltage regulator outputs a negative delta $\Delta i_d$, which is added to the $i_d$ component from the MTPA block. This action is to move the current vector to the left on the limit circle.

So, if $|v| \leq V_{lim}$, no action is taken; The PI controller output is positive so $\Delta i_d$=0. If $|v| > V_{lim}$, controller output becomes negative, and $\Delta i_d$ turns negative as well. This negative value is added to the $i_d$ reference.

Therefore, the reference $i_d$ of the current space vector is given by:

$$i_d = i_{dmTPA} + \Delta i_d$$

The minimum value $\Delta i_d$ is determined based on the starting current of the MTPV, typically $\Delta i_d min$= -300 for higher speeds for this motor speeds higher than 3650 rad/s a transition to Maximum Torque per Voltage (MTPV) mode takes place.

Then the transition happens to MTPV, in which using the MTPV derivations above I have

also implemented lookup table for Id and Iq on the MTPV trajectory based on the speed of the the motor, so the values of Iq and Id are calculated then if the modulus os Imtpv of Id and Iq is greater than the nominal current MTPV is ignored, otherwise it is a very high speed the requires the intervention of the MTPV trajectory, this switching between MTPA, FW, and MTPV was implemented with a matlab function shown below.

Listing 2.2: MTPA/FW/MTPV Function

```
function [Id, Iq] = fcn(IdFW, IdMTPA, we, weRef, Tref, IdMTPV, IqMTPV
   , I)
    Ld = 0.31e-3;
    Lq = 0.15e-3;
    lamex = 38.4e-3 * 3.8;
    P = 6;
    scaling_factor = Tref / 1177;

    if I > 736
        if we >= 1894
            if we <= 0.999 * weRef
                Id = IdMTPA + IdFW;
                Iq = sqrt(736^2 - Id^2) * scaling_factor;
            else
                Id = IdFW;
                Iq = Tref / (9 * ((Ld - Lq) * IdMTPA + lamex));
            end
        else
            Id = IdMTPA;
            Iq = Tref / (9 * ((Ld - Lq) * IdMTPA + lamex));
        end
    else
        Id = IdMTPV * abs(scaling_factor);
        Iq = IqMTPV * scaling_factor;
    end
end
```

the function takes all the required currents as an input, then based on the speed of the motor it assigns Id and Iq values, in which when the speed is lower than the base speed only MTPA is used then Iq is derived using the torque formula, and if it exceeds the base speed the FW current is added to MTPA current and Iq is chosen to be on the limit circle based on the new Id value, and then if the speed is very high Id and Iq are chosen to be the MTPV value, and they

are multiplied by this scaling factor to gradually be changed to zero when the reference speed is finally reached.

### 2.5.3 Current Control Loops

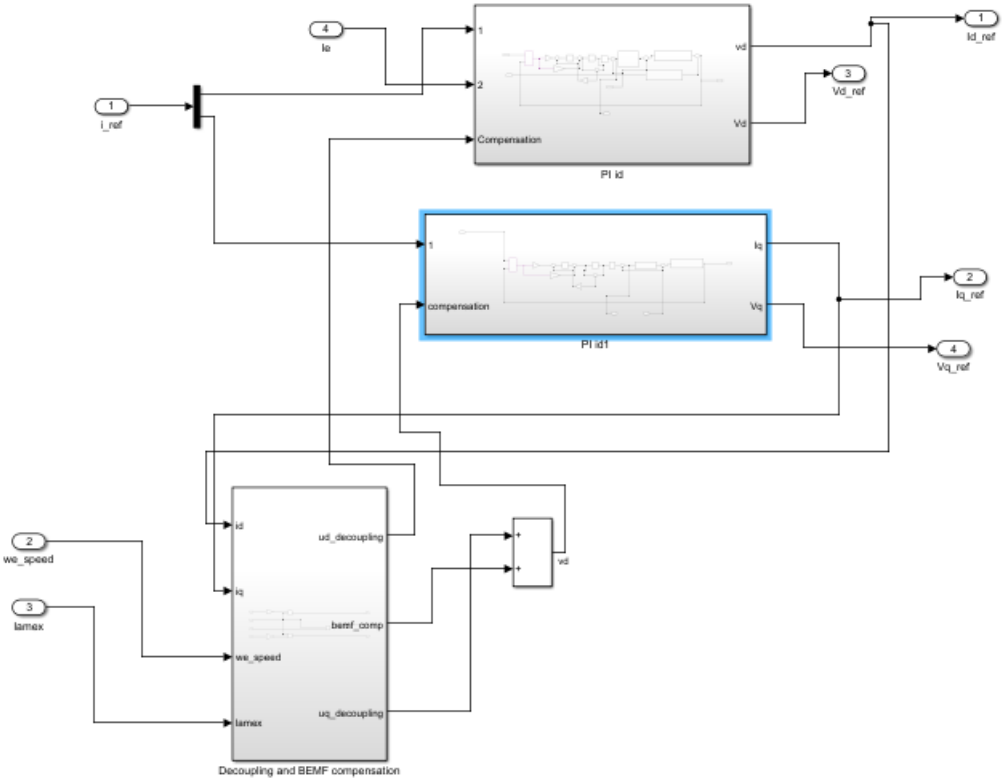


Figure 2.18: Current Control Block

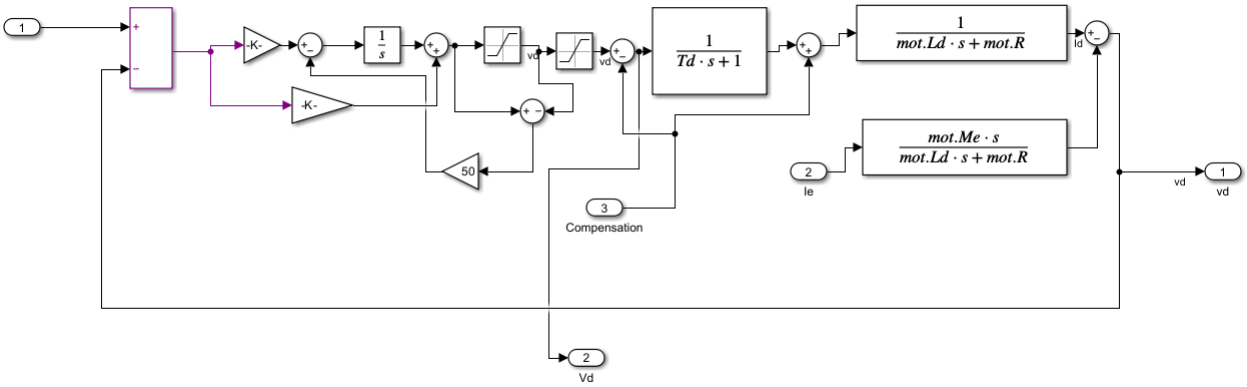


(a) d-axis current control block

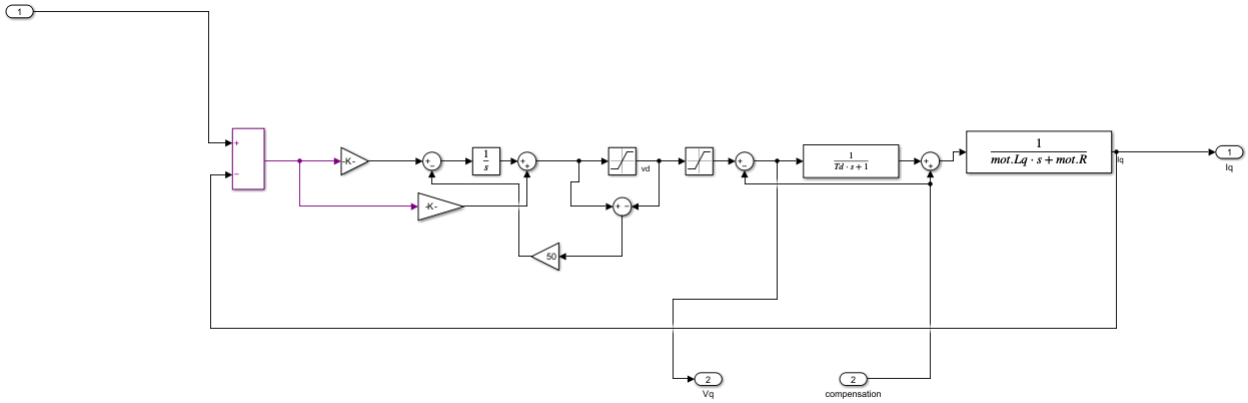


(b) d-axis current control block

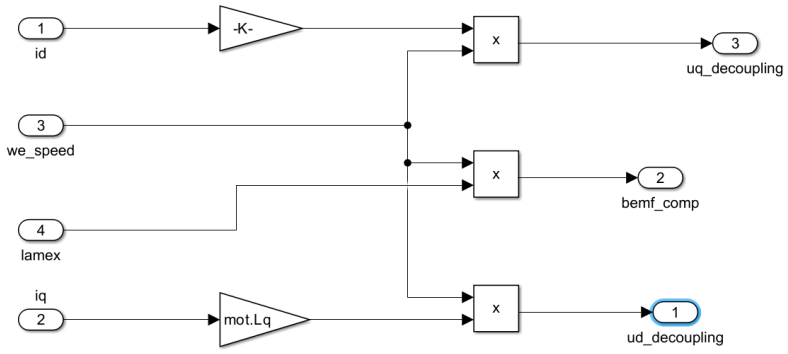


(c) d-axis Current Control Loop

Figure 2.19: Compensation to be applied to the current control loops

Thes design of the PI controller was done as illustrated previously, but the design was based on the voltage equations of the motor that was assumed to be linear.

$$u_d = R_s i_d + \frac{d\psi_d}{dt} - \omega_e \psi_q, \tag{2.35}$$

$$u_q = R_s i_q + \frac{d\psi_q}{dt} + \omega_e \psi_d, \tag{2.36}$$

then

$$u_d = R_s i_d + L_d I_d + L_m I_e s - \omega_e L_q I_q, \tag{2.37}$$

then

$$i_d(R_s + L_d s) = u_d - L_m I_e s + \omega_e L_q I_q, \tag{2.38}$$

finally,

$$i_d = \frac{u_d - L_m I_e s + \omega_e L_q I_q}{R_s + L_d s}, \tag{2.39}$$

but as mentioned above the design of PI controller only included the $u_d$ after the inverted block with $\frac{1}{R_s + L_d s}$, so the other terms weren't included in the design so they need to be subtracted from the voltage after the design is complete that is why the compensation are added, and the same is applied on the Iq control in which

$$u_q = R_s i_q + \frac{d\psi_q}{dt} + \omega_e \psi_d, \tag{2.40}$$

these are the equations used, in which after Laplace transform

$$u_q = R_s i_d + \psi_q s - \omega_e \psi_q, \tag{2.41}$$

then

$$u_q = R_s i_q + L_q I_q s + \omega_e L_d I_d, \tag{2.42}$$

then

$$i_q(R_s + L_q s) = u_q - \omega_e L_d I_d, \tag{2.43}$$

finally,

$$i_q = \frac{u_q - \omega_e L_d I_d}{R_s + L_q s}, \tag{2.44}$$

So here a compensation needed in which $\omega_e L_d I_d$ should be added to compensate with the simplified design that was done for the controller. The control blocks of both Id and Iq are shown in the figures above with he compensations taken into consideration. And exactly the same calculation is done also for Ie current which have a very near control scheme but with dependence on $R_e$ and $L_e$ instead of the stator resistance and d or q inductance.

### 2.5.4 Mechanical Model and Speed Block

After finding the current we enter the mechanical model in which the torque is now calculated based on the torque equations illustrated before, and from that torque value mechanical speed can be derived.

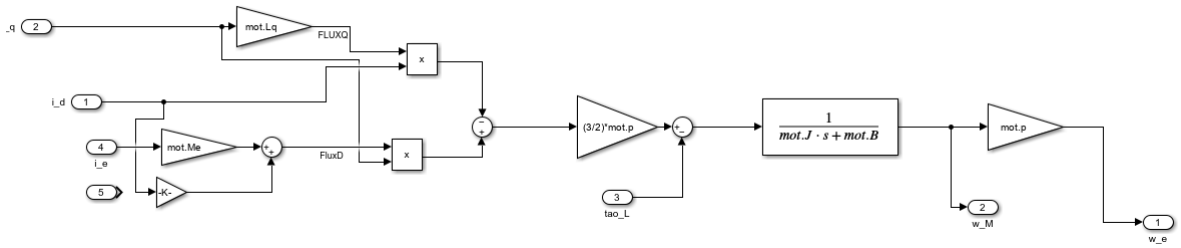


Figure 2.20: Mechanical Model and Speed Block

The mechanical speed response to an input torque can be modelled using a transfer function block $\frac{1}{Js+B}$. This block displays the relationship of the input torque, $T$, against the output angular speed, $\omega$. Where $J$ is the moment of inertia of the motor and $B$ is the damping coefficient.

A torque, $T$, being applied to the motor, the following dynamic equation may be used in characterizing the system:

$$J\frac{d\omega}{dt} + B\omega = T$$

Taking the Laplace transform of this equation, assuming zero initial conditions, we get:

$$Js\Omega(s) + B\Omega(s) = T(s)$$

where $\Omega(s)$ is the Laplace transform of the angular speed $\omega(t)$, and $T(s)$ is the Laplace transform of the input torque $T(t)$. Solving for $\Omega(s)$, we obtain:

$$\Omega(s) = \frac{T(s)}{Js + B}$$

Thus, the transfer function from input torque to the angular speed output is:

$$\frac{\Omega(s)}{T(s)} = \frac{1}{Js + B}$$

This transfer function, $\frac{1}{Js+B}$, implies that mechanical speed, $\omega$, is derived from the input torque, $T$, accounting for the inertias and dampings. Thus, the block $\frac{1}{Js+B}$ essentially transforms the input torque into an angular speed output, showing dynamic motor speed responses with respect to the torque applied. This is then multiplied by the number of motor poles to obtain electrical speed: mechanical speed x number of poles.

## 2.6 Simulation Results

On this section, the obtained results with the linear model of the motor will be visualized.

### 2.6.1 MTPA Region

On the MTPA control part, speed responses will be shown on when the speed in lower than the base speed, also the effect of anti-windup will discovered.

#### Speed Responses

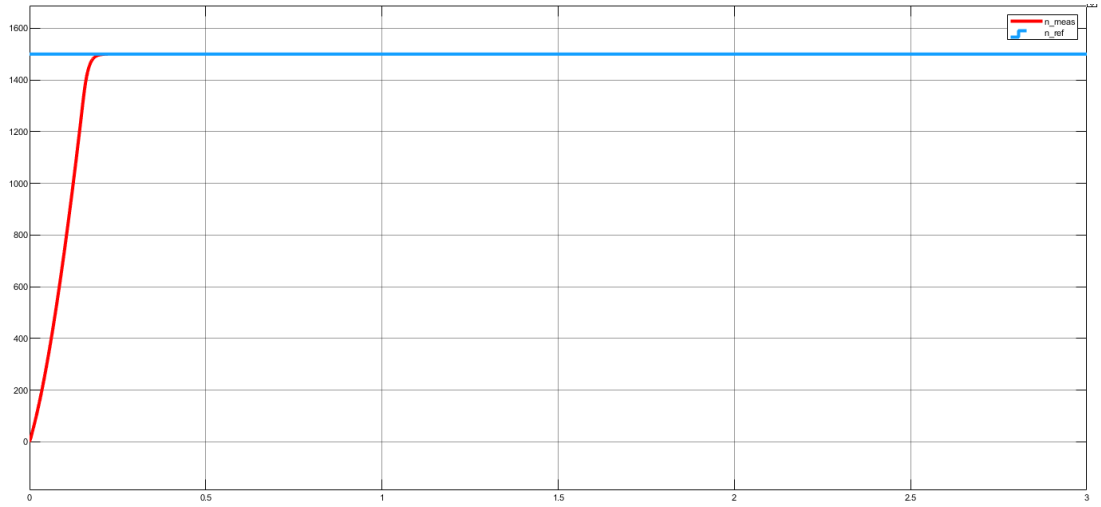


Figure 2.21: Speed Response with 1500 rad/s reference

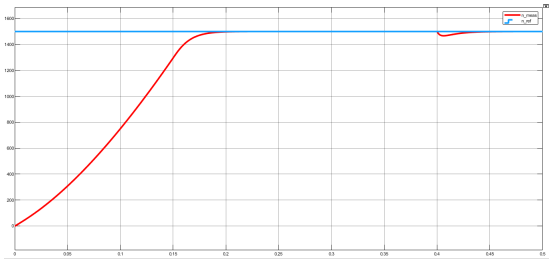

(a) TL = 1000 Nm

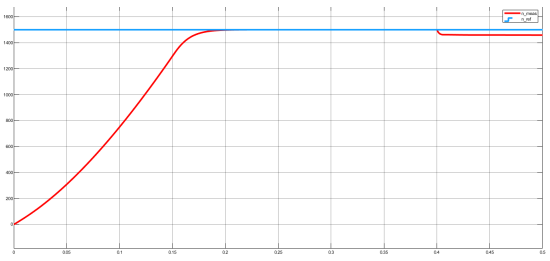

(b) TL = Nominal Torque

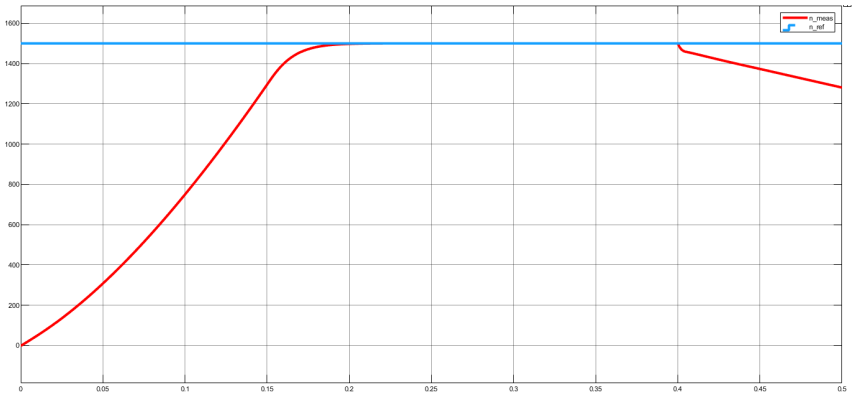


(c) TL = 1300 Nm (Bigger than Max Torque)

Figure 2.22: Speed Response with a reference of 1500 rad/s with different Load Torque values

As seen in the figures above the speed control was working perfectly well, in figure 21 the speed settled in a fast time and there were almost no overshoots thanks to the anti-windup. Moreover, in figure 22, it was shown that when the load torque was applied it also was able to track again as the load torque is smaller than the maximum torque, then it explodes if the load torque exceeds the maximum torque which is what we expect.

**Current Response**

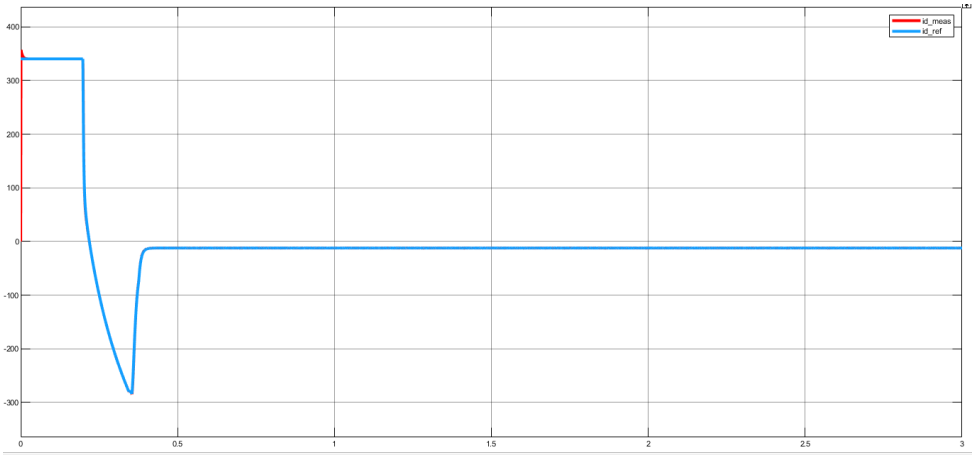


(a) Id Response

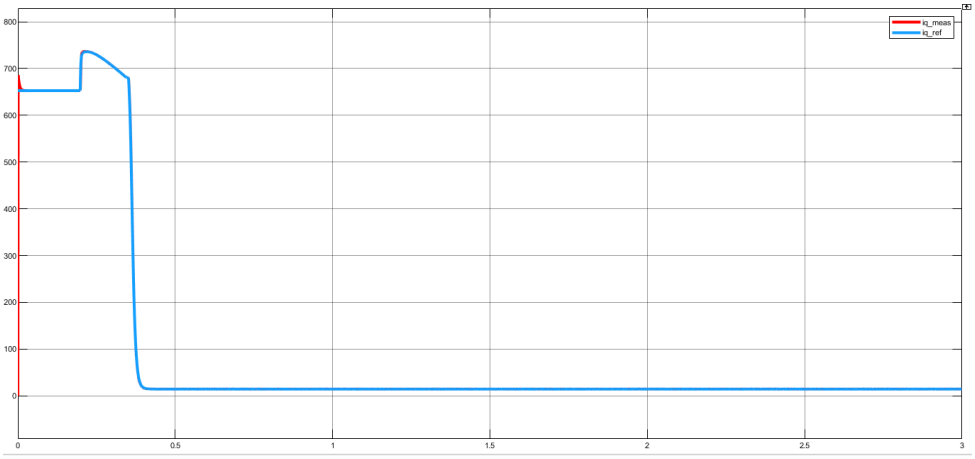


(b) Iq Response

Figure 2.23: Current Control References at 3400 rad/s speed reference

As shown here in figure 23 the current responses were very good, in which Id and Iq had every fast settling time with a small overshoot, then they tracked the reference coming from MTPA block perfectly, and then when the reference speed is reached they settled on zero.

**Current Variation during the Control**

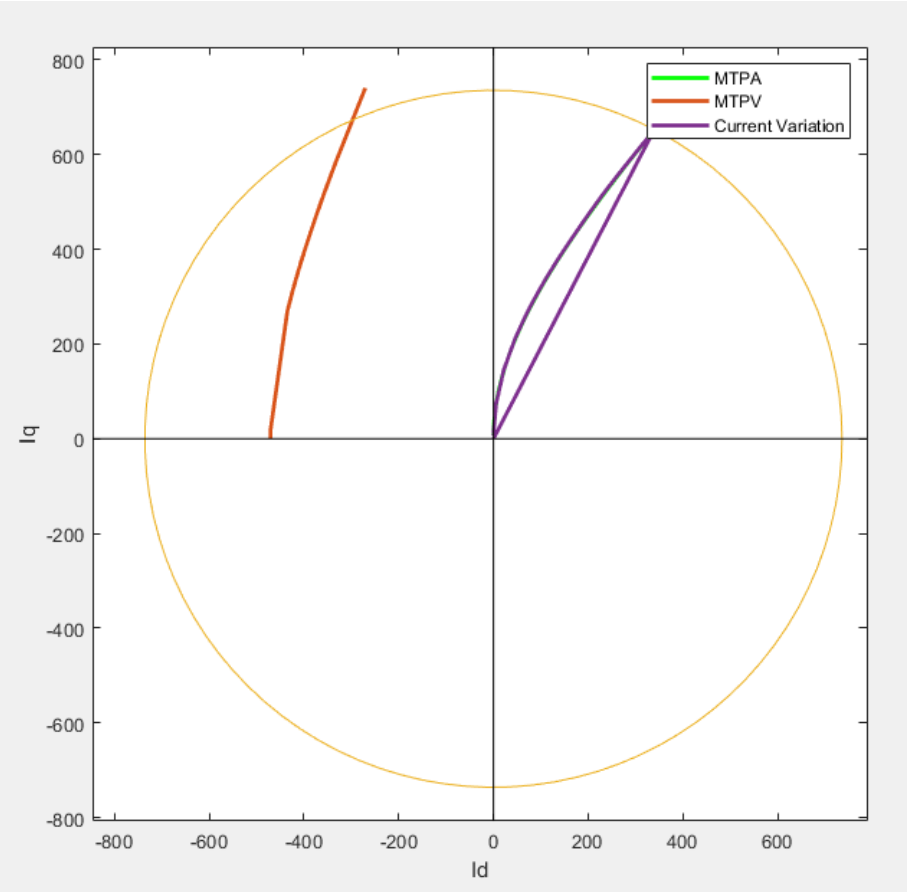


Figure 2.24: Current Variation with 1500 rad/s speed reference

As seen here in Figure 24 when the reference speed is lower than the base speed, the current only works on the MTPA trajectory then it comes back to zero when the response settles at the reference speed value.

### 2.6.2 FW Region

In this part, the results of the speed and current control will be shown when the reference speed is higher than the base speed but not very high to enter into MTPV control.

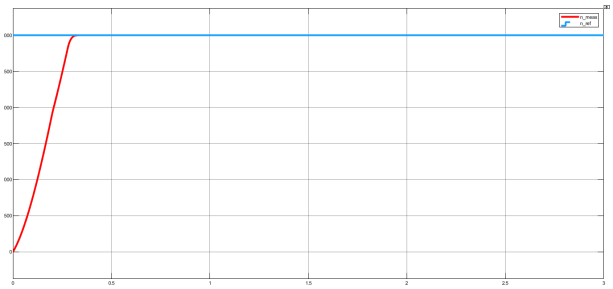

Figure 2.25: Speed Response with reference speed of 3000 rad/s

As in the MTPA part the speed is also perfectly tracking the reference with no issues.

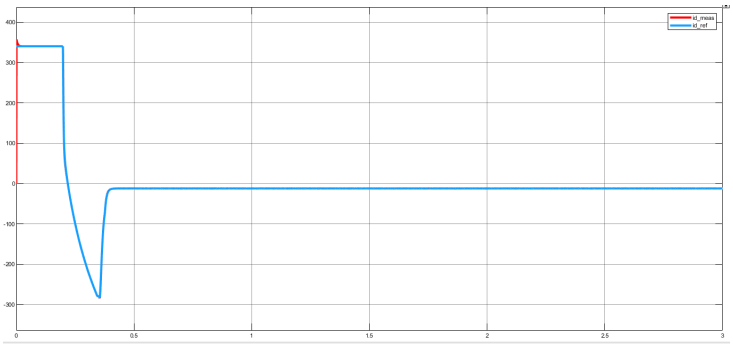

(a) Id Response

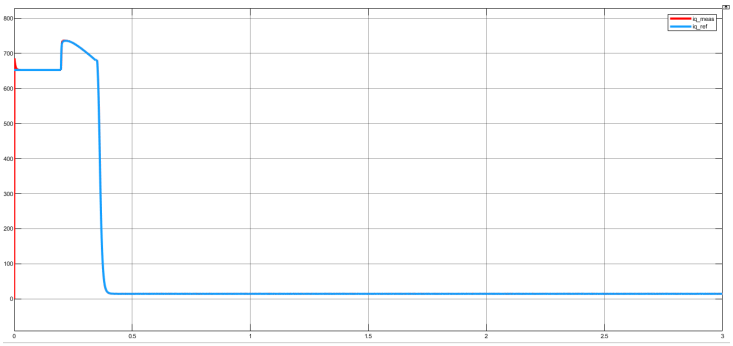

(b) Iq Response

Figure 2.26: Current Control References at 3400 rad/s speed reference

also, the current control was perfect, in which the response was fast and the tracking was perfect, where the recurrent behaviour was as expected in which Id decreased due to the flux weakening.

**Current Behaviours During FW**

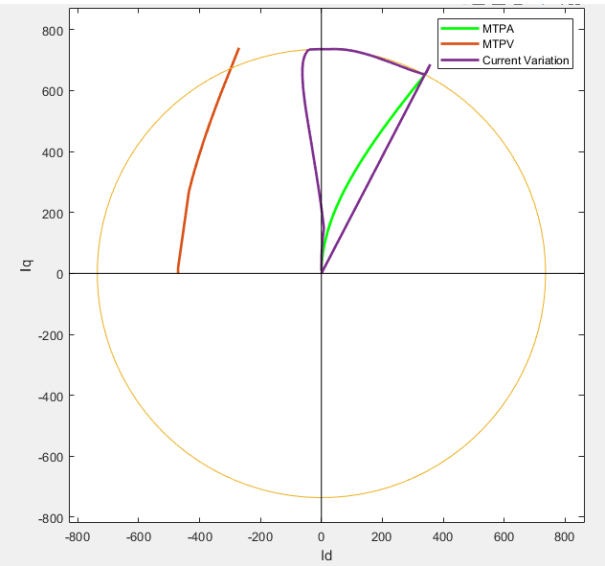


(a) Reference Speed 2400 rad/s

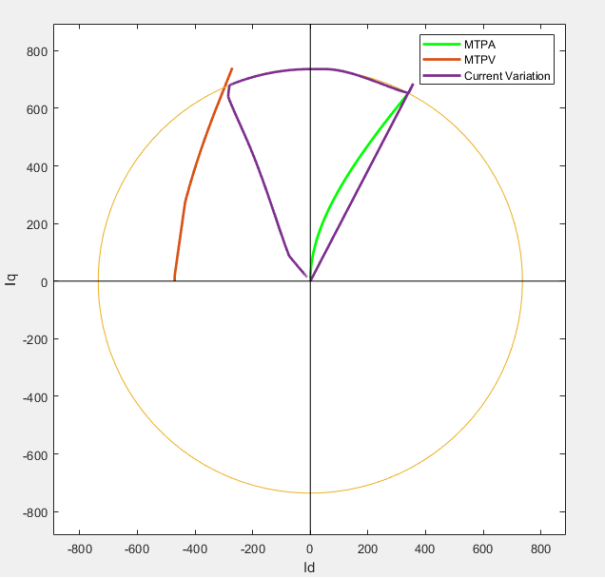


(b) Reference Speed 3400 rad/s

Figure 2.27: Current Control behaviour During FW

As shown in the figure as the speed goes beyond the base speed, FW region starts, in which the current vector in shifted to the left on the limit circle before the need to enter the MTP trajectory.

### 2.6.3 MTPV Region

In this part the speed is now very high, with the linear model a speed of 9900 rad/s was able to be achieved, this speed is around 6.3 times the base speed, which is very high. As shown in the

figure below the speed was perfectly tracked after 2.75 seconds with no overshoot. As for the current the tracking was perfect as before.

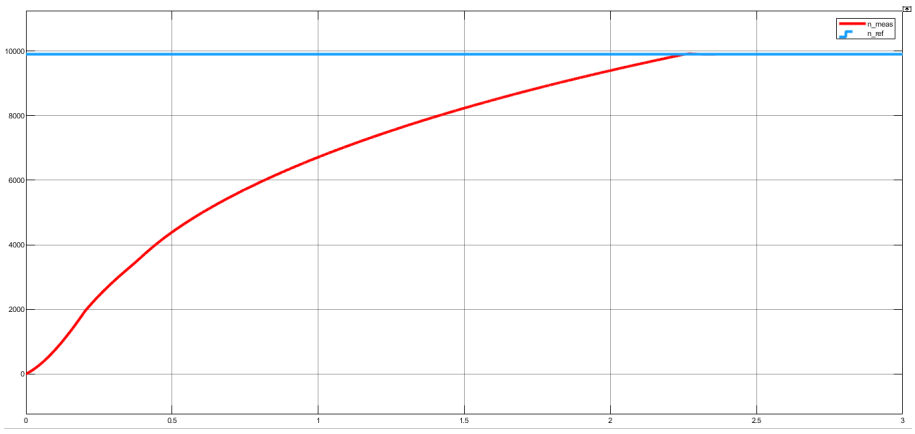


Figure 2.28: Maximum Speed Achieved

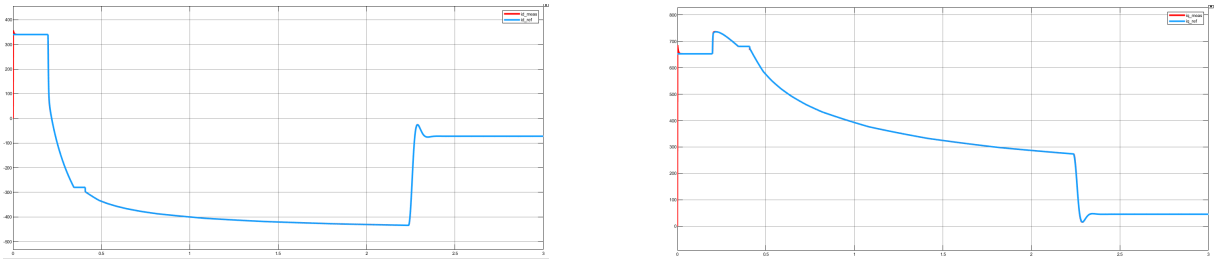

(a) Id Response

(b) Iq Response

Figure 2.29: Current Control References at 3400 rad/s speed reference

**Current Behaviour with MTPV**

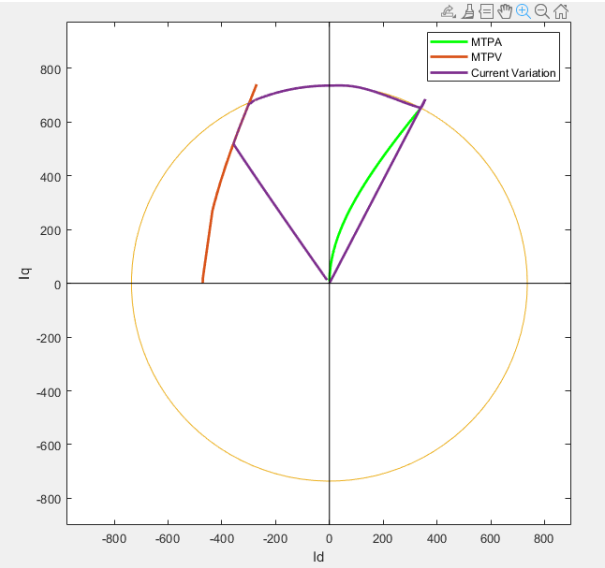


(a) Reference Speed 5000 rad/s

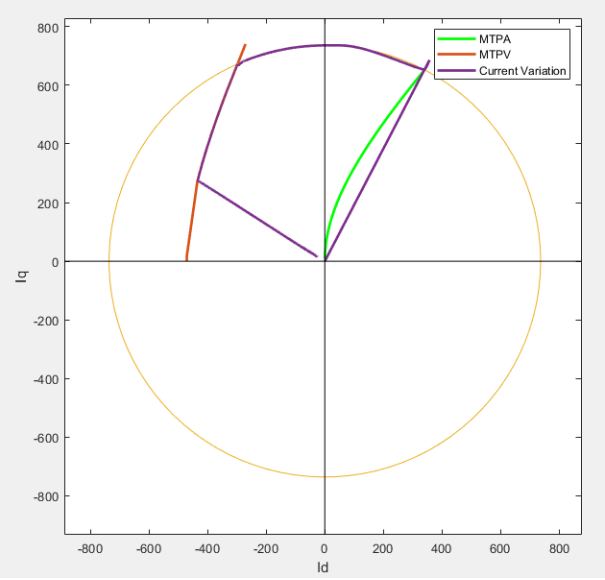


(b) Reference Speed 9900 rad/s

Figure 2.30: Current Control behaviour During MTPV

Here as seen here in the figure as the speed increase we enter to the FW region then to MTPV region, and as speed increase we go deeper in the MTPV trajectory.

### 2.6.4 Effect of Anti-windup

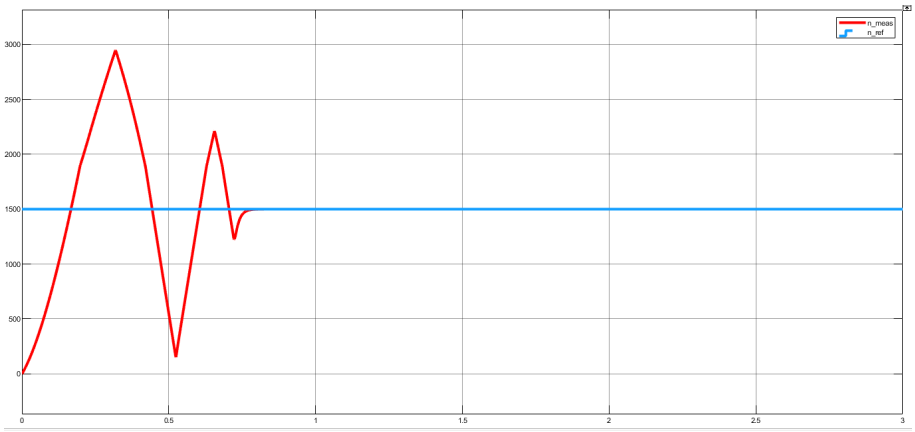


Figure 2.31: Speed Response with 1500 rad/s reference with no ati-windup

As shown in the figure if I used the same gains calculated with the bode method a massive overshoot would occur, this ensures how important is to use anti-wind up for the control of the motor. Without the anti-windup, the motor will not operate at high speeds.

# Chapter 3

# Non-Linear Model of Hybrid Excited Permanent Magnet Motor

## 3.1 Non-linearities of EESM

Electrically excited synchronous motor drives have inherent nonlinearities, most of which seriously affect performance and control. Their biggest source of nonlinearity is magnetic saturation, occurring when the core materials reach their maximum magnetic flux capacity, hence delivering a nonlinear relation between current and magnetic flux. Furthermore, magnetic cross-coupling of the fluxes on the d axis and q axis introduces dynamic interactions, whereby changes on one axis impact the other and hence complicate motor behavior even more. Non-linear voltage and current distortions are introduced into the motor due to eddy currents and hysteresis losses at its iron core, while variable inductances caused by variations in rotor position and excitation current result in non-linear inductance profiles. Iron losses, which include hysteresis and eddy current losses, are frequency-dependent and add to the non-linear characteristics of the motor. The current-to-flux linkage relationship is inherently non-linear, influenced by the magnetic material properties and motor design. The skin effect at high frequencies causes non-uniform current distribution, increasing effective resistance and decreasing inductance, thus introducing non-linear frequency-dependent effects. It also includes many more nonlinearities coming from magnetic reluctance variations, back-EMF distortions, or nonlinear control elements like saturation limits or nonlinear PI controllers, all adding to the general nonlinearity of the EESM. The ability to accommodate these nonlinearities appropriately within modeling and control methods for very high accuracy in modeling and effectiveness in control usually entails advanced techniques like FEA and LUT methods that enable the capturing of these effects comprehensively for improved performance in motor drive systems. [17].

## 3.2 Dynamic Modeling Approaches

### 3.2.1 Flux-Linkage Based Models

Flux-linkage-based models use the flux linkage as the state variable and require the inversion of the current-to-flux linkage characteristics. These models are highly detailed but computationally intensive due to the need to handle nonlinear mappings between current and flux linkage. Primary advantages of flux-linkage models are that they can express magnetic behavior of the motor in great detail, which enables applications like detailed simulations and advanced control strategy development. [18].

### 3.2.2 Current-Based Models

In current-based models, however, the stator current is used as the state variable, and thus the need for inversion of the current-to-flux linkage maps is avoided. For such models, computation of incremental inductances will be required—the derivatives of flux linkage with respect to the stator currents. Very often, current-based models become simplistic in implementation and potentially computationally more efficient—hence quite feasible for all real-time control-oriented applications [18].

## 3.3 Proposed Current-Based Dynamic Model for EESM

### 3.3.1 Model Formulation

The voltage-balance equations in the dq reference frame aligned with the rotor position can be used to describe dynamic behavior of the EESM as:

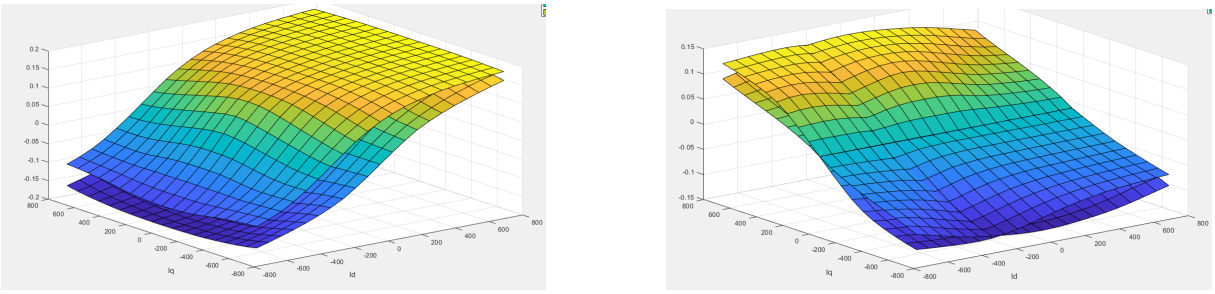

(a) FLux Linkage d

(b) Flux linkage q

Figure 3.1: Flux Linkage maps as a function of currents Id and Iq

$$\begin{aligned}
\frac{d\lambda_d(i_d, i_q, i_e)}{dt} &= u_d - R_s i_d - \omega_e \lambda_q(i_d, i_q, i_e), \\
\frac{d\lambda_q(i_d, i_q, i_e)}{dt} &= u_q - R_s i_q + \omega_e \lambda_d(i_d, i_q, i_e), \\
\frac{d\lambda_e(i_d, i_q, i_e)}{dt} &= u_e - R_e i_e,
\end{aligned} \tag{3.1}$$

The flux linkages can be expressed as a function of the currents in such a way that it would more accurately model the nonlinearities, including the iron saturation effect and magnetic cross-coupling. It is nonlinear behavior, which is captured by computing the incremental inductances, actually the partial derivatives of flux linkages concerning the currents.

$$L(i) = \frac{d\lambda(i)}{di} \tag{3.2}$$

The current-based model can then be expressed in a matrix form, highlighting the dependencies of the flux linkages and currents:

$$\frac{d\lambda(i)}{dt} = L(i)\frac{di}{dt} = u - Ri - \omega_e J\lambda(i) \tag{3.3}$$

where $L(i)$ is an incremental inductance matrix, while $J$ is skew-symmetric, owing to cross-coupling between the d and q axes, and $R$ is a resistance matrix. The incremental inductance matrix is defined here as the Jacobian matrix of the flux linkage vector with respect to the current vector. This Jacobian, for the EESM, may be written as:

$$L(i) = \begin{bmatrix} \frac{\partial \lambda_d}{\partial i_d} & \frac{\partial \lambda_d}{\partial i_q} & \frac{\partial \lambda_d}{\partial i_e} \\ \frac{\partial \lambda_q}{\partial i_d} & \frac{\partial \lambda_q}{\partial i_q} & \frac{\partial \lambda_q}{\partial i_e} \\ \frac{\partial \lambda_e}{\partial i_d} & \frac{\partial \lambda_e}{\partial i_q} & \frac{\partial \lambda_e}{\partial i_e} \end{bmatrix} \tag{3.4}$$

The computation of this matrix requires the partial derivatives of flux linkages $\lambda_d$, $\lambda_q$, and $\lambda_e$ with respect to $i_d$, $i_q$, and $i_e$. These partial derivatives are derived from the results of finite element analysis (FEA).

Finite element analysis is used to develop an accurate map of flux linkages as functions of currents. Drawing an accurate motor geometry and creating a grid in the available $i_d$-$i_q$ axis plane, my colleague applied, for each grid point, the phase currents $i_{ax}$, $i_{bx}$, and $i_{cx}$ and ran simulations to calculate the flux linkages.

Then these maps were used to find the partial derivative to be enabled to find and fill the L matrix by interpolation. the derivatives were calculated using Matlab by differentiating the fluxes on the acquired maps by the currents. the map of the acquired inductance.

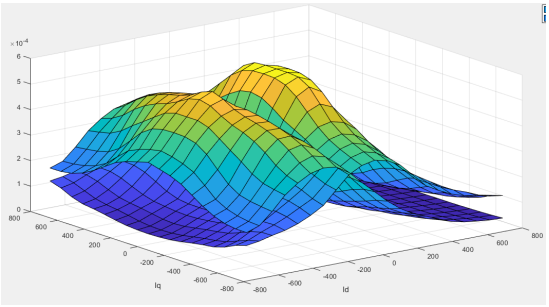

(a) Ldd

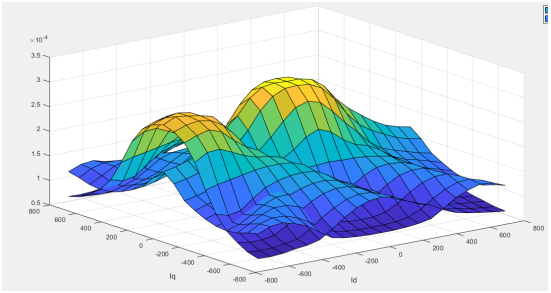

(b) Lqq

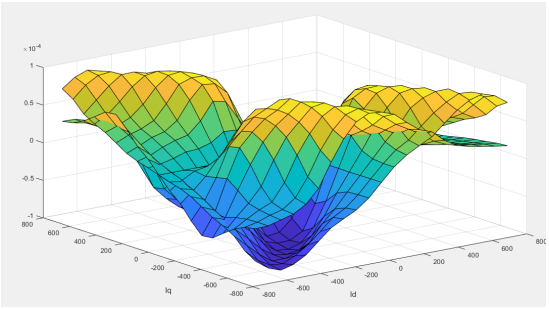

(c) Ldq

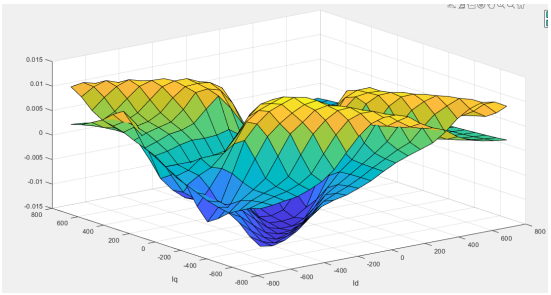

(d) Lqe

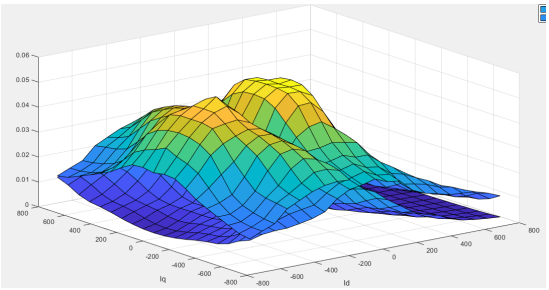

(e) Lde

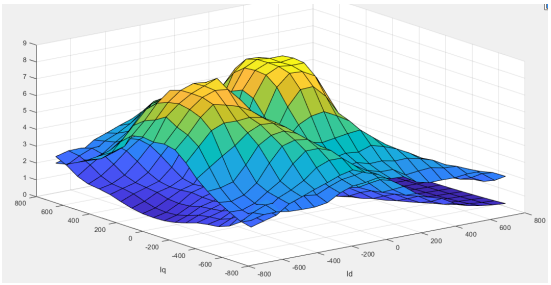

(f) Lee

Figure 3.2: Inductance maps with the minimum and maximum value of $I_e$

### 3.3.2 Non-linear Current model of the motor

Then, after being able to find the L matrix and using equation 2.3 above, as shown in the coming figure, I will have the final model of the model where I will have the voltages issued from the controllers as an input, and the currents will be the output of this model.

## 3.4 Simulink Model

The model decision blocks are the same but with slight changes, in which now we have to use the current model above to consider the non-linearaties, so the current loop output will only be the voltage that will enter an inverter to enter the non-linear model of the motor in which

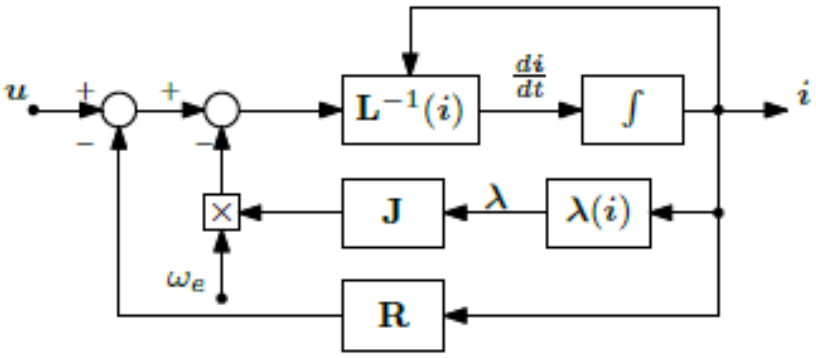


Figure 3.3: Current Model of the Motor

the currents will be calculated and returned as feedback to the current loops. below only the changed parts of the model will be introduced and the other blocks will remain as was explained in the linear Part.

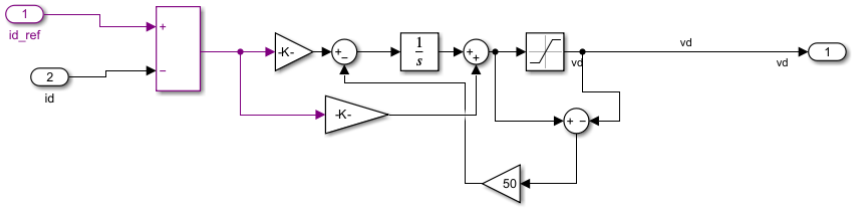


Figure 3.4: Iq and Id current Lopps

Both Id and Iq current control loops will be exactly the same as this simple model, in which vd and vq will be the output control signal based on the error.

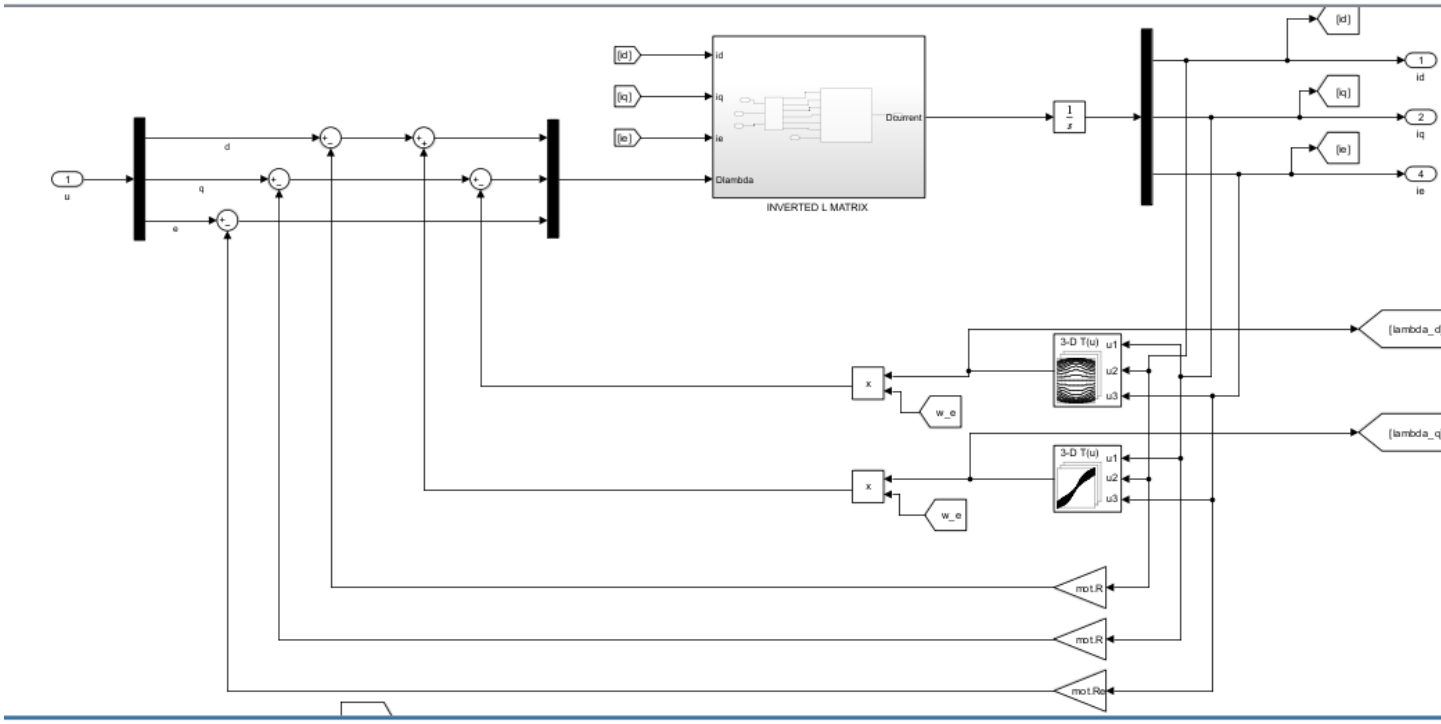


(a) FLux Linkage d

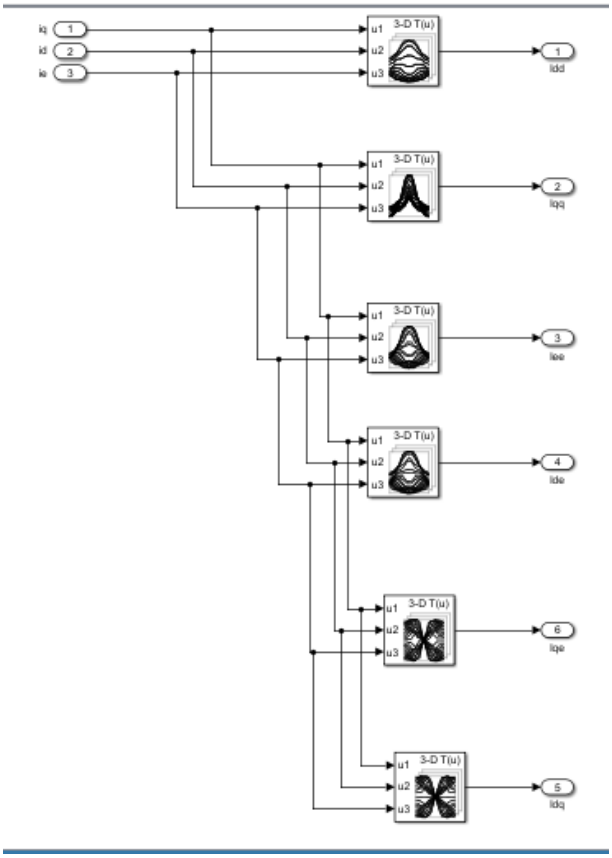


(b) Flux linkage q

in the figure above the Non-linear model of the motor discussed in the previous section was

implemented on Simulink, in which the flux linkage are interpolated from the LUTs that where implemented using the maps calculated before, after calculating all the inductances they are entered to the Matrix L using this Matlab function.

Listing 3.1: I calculation

```
function Dcurrent= fcn(ldd, lqq, lee, lde, ldq, lqe, Dlambda)

l_diff= zeros(3,3);
l_diff(1,1)=ldd;
l_diff(1,2)=ldq;
l_diff(1,3)=lde;

l_diff(2,1)=ldq;
l_diff(2,2)=lqq;
l_diff(2,3)=lqe;

l_diff(3,1)=(3/2)*lde;
l_diff(3,2)=(3/2)*lqe;
l_diff(3,3)=lee;

linv_diff=inv(l_diff);

Dcurrent=linv_diff*Dlambda;

end
```

in which matrix L is filled this way, then this matrix is inverted, then multiplied by Dlamda which was calculated using the equations above. then we have di/dt, then this value is integrated to acquire finally the values of the currents.

### 3.4.1 Simulation Results

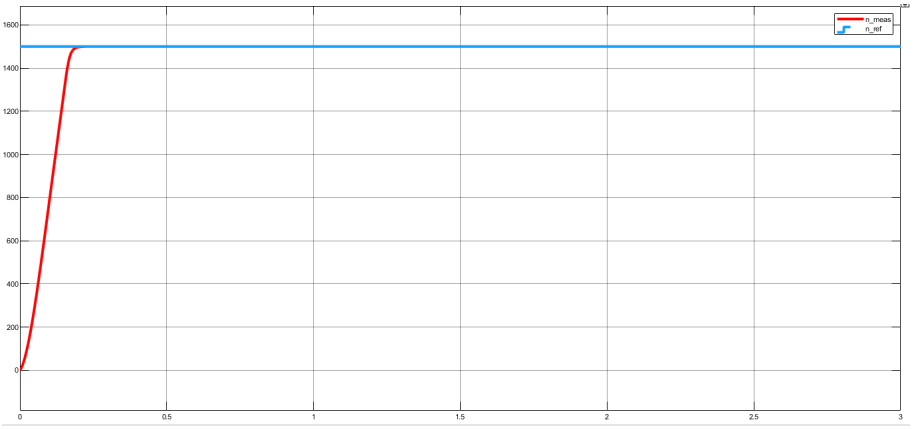


Figure 3.6: Speed Response with reference of 1500 rad/s

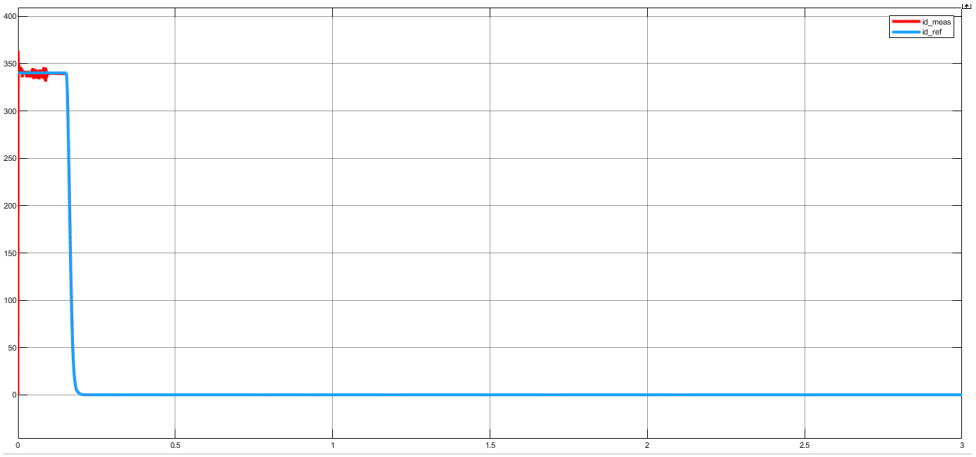


(a) Id Response

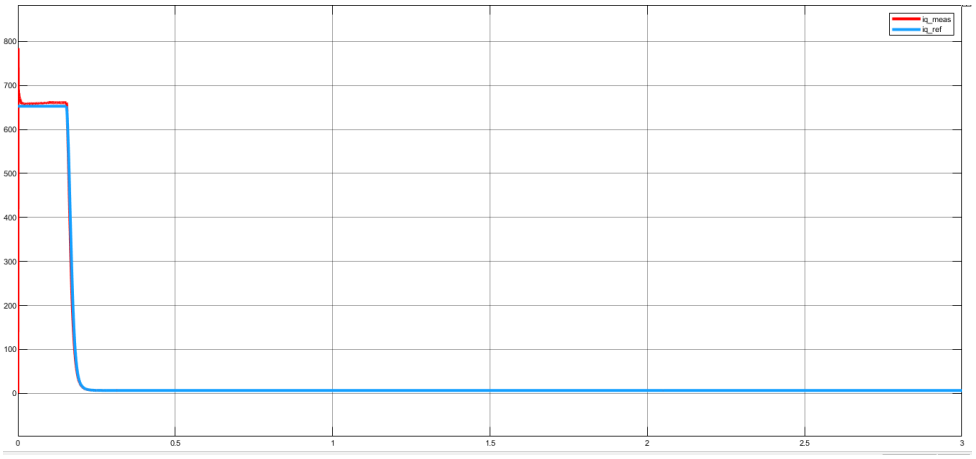


(b) Iq Response

Figure 3.7: Current Control References at 1500 rad/s speed reference

Here in the figures, the responses were similar to the results achieved with the linear model of the motor, but currents show a higher overshoot at the beginning.

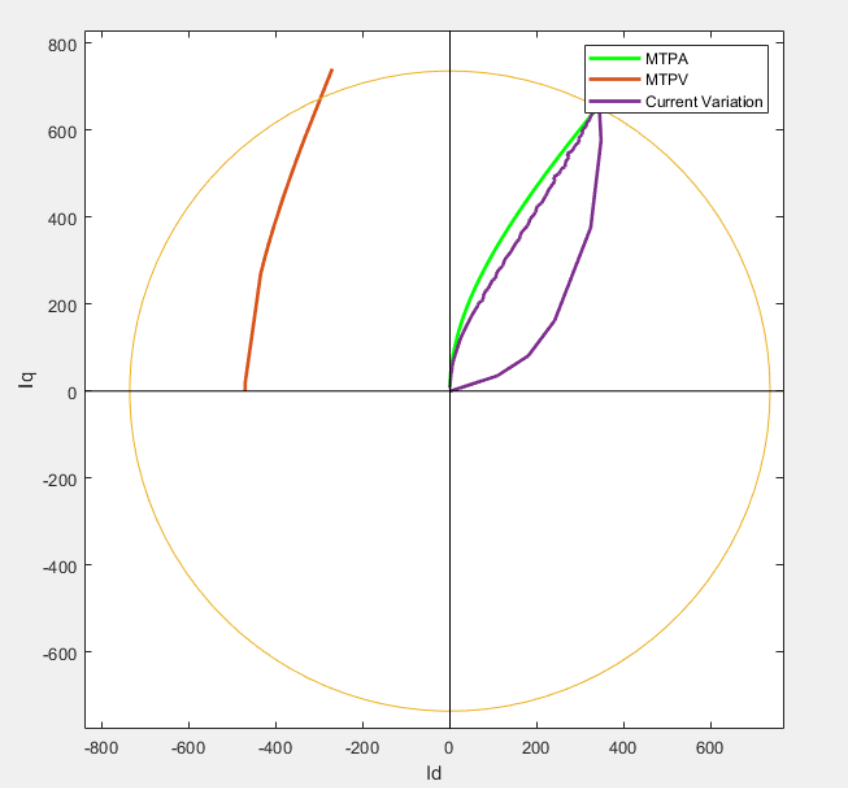


Figure 3.8: Current Variation with 1500 rad/s reference

Here as shown the current varies with the MTPA trajectory, but it doesn't exactly match the trajectory like in the linear case, but it is considered very close.

### 3.4.2 Simulation Results

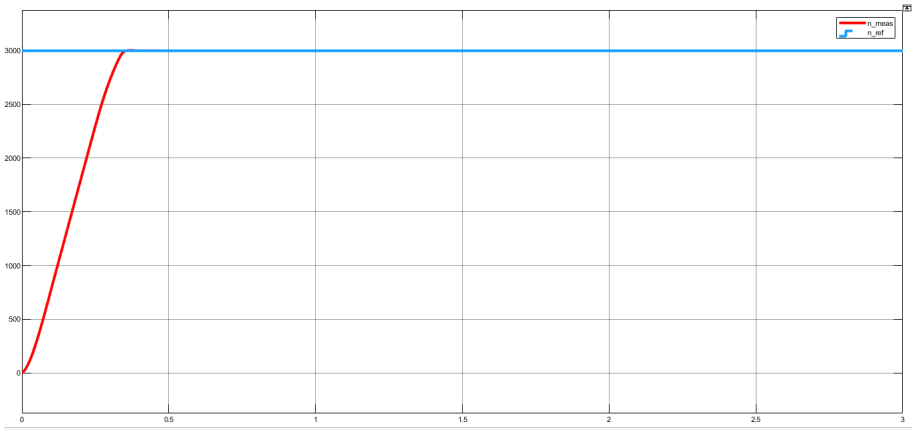


Figure 3.9: Speed Response with reference of 3000 rad/s

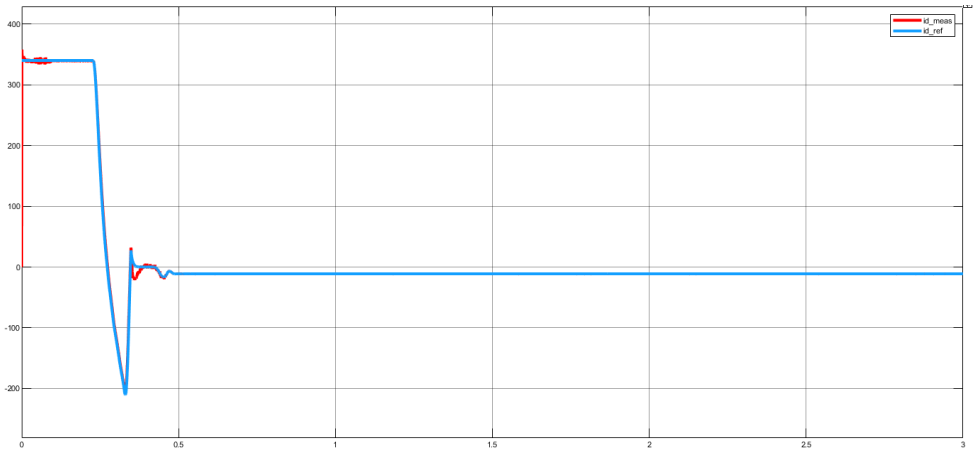


(a) Id Response

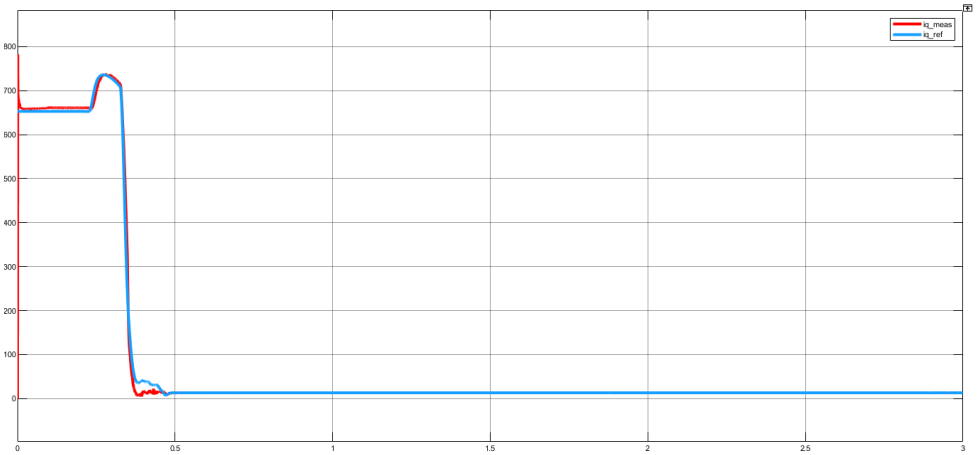


(b) Iq Response

Figure 3.10: Current Control References at 1500 rad/s speed reference

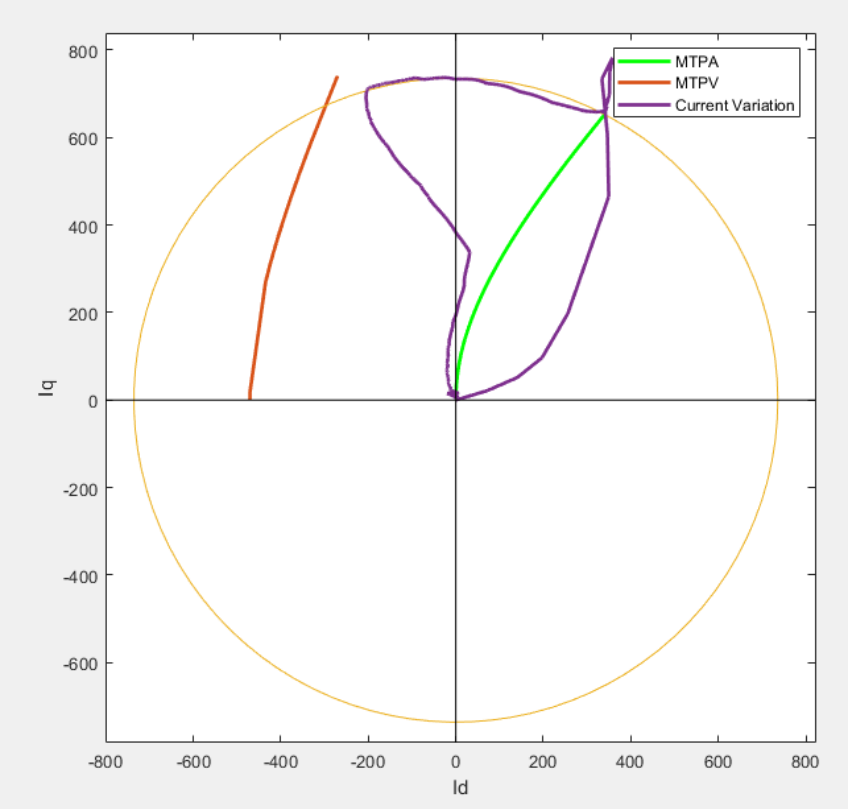


Figure 3.11: Current Variation with 3000 rad/s reference

Finally, a very good results were achieved also with the non-linear model in both MTPA and FW regions, where the speed was able to track the reference perfectly so was the current, the behaviour of the non-linear motor is a big tricky, which when the speed enters very high speed, the motor was able to reach the speed but it was very hard to control it so it explodes when it reaches the reference speed.

## 3.5 conclusion

This thesis describes the high-level control strategies of EESM, with detailed implementation and optimization of flux-weakening control. Testing involved the design and integration of control strategies like MTPA, flux weakening, and MTPV, showing their effectiveness in improving the performance and efficiency of EESMs under a wide range of operational scenarios. The research began with a deep literature review and hastened to disclose the great benefits that EESMs have over their traditionalPermanent Magnet Synchronous Motor counterparts, particularly in controllability and adaptability for a very wide scope of applications, among them electric vehicles, industrial drives, and renewable energy systems. The unique configuration of EESMs, which allows for effective control of rotor field current, was identified as a key factor in

their superior performance capabilities in which a very high speed compared to the permanent magnet motors could be achieved. In the further sections, a robust control algorithm integrating the MTPA, flux weakening, and MTPV strategies was developed. It is carefully designed to make EESMs efficient with high torque output by automatically adapting to different loaded conditions and speed. A detailed mathematical modeling and subsequent analysis came up with a solid theoretical framework of this control algorithm. The proposed control strategies were tested through extensive simulation studies. From these simulations, it was obvious that the integrated control algorithm could significantly improve the operational efficiency of EESMs, especially under high-speed and high-torque conditions. In this thesis, the main contribution was to design a fractional-order speed controller and develop a detailed integrated control algorithm by combining MTPA, Flux Weakening, and MTPV strategies to provide an overall solution for the optimization of performance of the EESM under different operational conditions. The theoretical and simulation analyses also showed a very good model of EESM control. To this regard, these findings of the study greatly improve electric motor control techniques by providing a robust framework for the efficient and reliable operation of EESMs. Several lines of future research are identified to further develop the capabilities and applications of these motors. To this respect, future work should consider the integration of more advanced control techniques, such as predictive or adaptive control, in order to further optimize the EESMs with respect to the varying operational conditions. Optimization of control for EESMs under uncertain and time-varying operating conditions would lead to a more resilient control strategy.

# Bibliography


[1] P. Su, W. Hua, Z. Wu, Z. Chen, G. Zhang, and M. Cheng, "Comprehensive comparison of rotor permanent magnet and stator permanent magnet flux-switching machines," *IEEE Transactions on Industrial Electronics*, vol. 66, no. 8, pp. 5862–5871, Aug. 2019.

[2] A. Ceban, R. Pusca, and R. Romary, "Study of rotor faults in induction motors using external magnetic field analysis," *IEEE Transactions on Industrial Electronics*, vol. 59, no. 5, pp. 2082–2093, May 2012.

[3] D.-Q. Nguyen, L. D. Hai, D. B. Minh, and V. D. Quoc, "Analysis of electromagnetic parameters of hybrid externally excited synchronous motors for electric vehicle applications," *Engineering, Technology & Applied Science Research*, vol. 13, no. 3, pp. 10 670–10 674, 2023.

[4] A. Dalal and M. Sreejeth, "Wide speed range control of pmsm based on mtpa and flux-weakening control," in *2023 International Conference on Power, Instrumentation, Control and Computing (PICC)*, Thrissur, India, 2023, pp. 1–6.

[5] S. Liu, Z. Song, B. Zhang, and C. Liu, "Flux weakening controller design for series-winding three-phase pmsm drive systems," *World Electric Vehicle Journal*, vol. 14, no. 4, p. 107, 2023.

[6] S. Liu, Q. Gao, Y. Teng, and D. Xu, "Mtpa control and flux-weakening control for ipmsm drives based on high-frequency signal injection," in *2023 IEEE 6th International Electrical and Energy Conference (CIEEC)*, Hefei, China, 2023, pp. 896–901.

[7] J. Tang, B. Jiang, L. Boscaglia, H. Chen, and Y. Liu, "Observations of field current and field winding temperature in electrically excited synchronous machines with brushless excitation," in *2022 International Conference on Electrical Machines (ICEM)*, Valencia, Spain, 2022, pp. 841–847.

[8] S. Akbar, F. Khan, W. Ullah, B. Ullah, A. H. Milyani, and A. A. Azhari, "Performance

analysis and optimization of a novel outer rotor field-excited flux-switching machine with combined semi-closed and open slots stator," *Energies*, vol. 15, no. 20, p. 7531, 2022.

[9] F. Liu, X. Wang, and Z. Xing, "Design of a 35 kw permanent magnet synchronous motor for electric vehicle equipped with non-uniform air gap rotor," *IEEE Transactions on Industry Applications*, vol. 59, no. 1, pp. 1184–1198, Jan.-Feb. 2023.

[10] H. Wu, J. Zhao, T. Shen, and Z. Wang, "Research on mtpa control strategy based on dpwm and svpwm integrated modulation," in *2023 8th Asia Conference on Power and Electrical Engineering (ACPEE)*, Tianjin, China, 2023, pp. 1562–1571.

[11] R. Mbayed, G. Salloum, L. Vido, E. Monmasson, and M. Gabsi, "Hybrid excitation synchronous generator in embedded applications: Modeling and control," *Mathematics and Computers in Simulation*, vol. 90, pp. 60–73, 2013.

[12] S. Akbar, F. Khan, W. Ullah, B. Ullah, A. H. Milyani, and A. A. Azhari, "Performance analysis and optimization of a novel outer rotor field-excited flux-switching machine with combined semi-closed and open slots stator," *Energies*, vol. 15, p. 7531, 10 2022.

[13] S. Jia, P. Sun, S. Feng, D. Liang, and X. Dong, "A novel stator-pm consequent-pole dual stator/rotor armature winding flux modulated machine for multi-torque components," in *2022 IEEE 20th Biennial Conference on Electromagnetic Field Computation (CEFC)*, Denver, CO, USA, 2022, pp. 1–2.

[14] J. Pyrhonen, *Design of Rotating Electrical Machines*, 2008.

[15] F. Husnayain, T. Noguchi, R. Akaki, and F. Yusivar, "Improved current and mtpa control characteristics using fem-based inductance maps for vector-controlled ipm motor," *Energies*, vol. 16, no. 12, p. 4712, 2023.

[16] Y. Lu, L. Zhu, S. He, H. Yang, H. Luo, and R. Zhao, "Newton downhill method based maximum torque per voltage control of ipmsm considering variation of motor parameters," in *2022 IEEE International Power Electronics and Application Conference and Exposition (PEAC)*, Guangzhou, Guangdong, China, 2022, pp. 606–611.

[17] Q.-M. Wu, Y. Zhan, M. Zhang, X.-P. Chen, and W.-P. Cao, "Efficiency optimization control of an ipmsm drive system for electric vehicles (evs)," *International Journal of Control, Automation and Systems*, vol. 19, no. 8, pp. 2716–2733, 2021.

[18] P. G. Carlet, L. Cinti, L. Ortombina, and N. Bianchi, "Dynamic model for hepm motors including the nonlinear magnetic characteristics," in *2023 IEEE International Electric Machines & Drives Conference (IEMDC)*, 2023.